Electronic Supplementary Information for Protecting Effect of Mass Transport during Electrochemical Reduction of Oxygenated Carbon Dioxide Feedstocks

Kindle Williams, Nathan Corbin, Joy Zeng, Nikifar Lazouski, Deng-Tao Yang, Karthish Manthiram

S.1 Materials

Carbon dioxide (CO_2; CD I200, Instrument grade, 99.99% purity for bubbling; CD R300, Research grade, 99.999% purity for CO_2 reduction experiments) and oxygen (O_2, OX 300, Industrial grade, 99.7% purity) were purchased from Airgas. Nitrogen (N_2) gas was available in-house and was generated by boiloff of liquid nitrogen from Airgas. High-pressure compressed air (used to dry cell parts and foils) was also available in-house and was compressed at MIT's on-campus power generation facility. Gold foils (Au, 00132, 0.127 mm (0.005 in) thick, *Premion*® 99.99% (metals basis) – Lot T13D021) and sodium formate (HCOONa, 36424, ACS, 99.0% min.) were purchased from Alfa Aesar. Platinum foils (Pt) were purchased both from Alfa Aesar (00262, 0.025 mm (0.001 in) thick, 99.9% (metals basis)) and from BeanTown Chemical (213815, 0.025 mm thick, 99.99% trace metals basis). Experimental reference electrodes (Leak-Free Ag/AgCl in 3.4 M KCl, model LF-2) were purchased from Innovative Instruments, Inc. The master calibration electrode (Ag/AgCl, CHI111) was purchased from CH Instruments, Inc. Selemion™ AMV anion exchange membranes were purchased from AGC Engineering Co. Ultra-pure water was produced on-site by a Milli-Q® Integral Water Purification System purchased through EMD Millipore. Deuterium oxide (D_2O, 426931000, for NMR, 99.8 atom % D, AcroSeal® – Lot A0380655) and potassium ferricyanide ($K_3Fe(CN)_6$, 223111000, 99+%, for analysis – Lot A0384569) were purchased from Acros Organics. Nitric acid (HNO_3, A509-P212, 67-70%, TraceMetal grade), sulfuric acid (H_2SO_4, A510-P212, 93-98%, TraceMetal grade), potassium chloride (KCl, P217-500, certified ACS – lot 166181), and dimethyl sulfoxide (DMSO, D139-1) were purchased from Fisher Scientific. Sodium carbonate (Na_2CO_3, 451614, anhydrous, powder, 99.999% trace metals basis – Batch 0000023782), sodium perchlorate ($NaClO_4$, 410241, ACS reagent, ≥98.0% - Lot MKCC2028), phenol (328111, unstabilized, purified by redistillation), methanol (322415, anhydrous, 99.8%), ammonium molybdate tetrahydrate ($(NH_4)_6Mo_7O_{24}$, 431346, ACS reagent, 99.98% trace metals basis – Lot MKCD1517), and hydrogen peroxide (H_2O_2, 216763, contains inhibitor, 30 wt % in H_2O, ACS reagent – Lot MKBX1362V) were purchased from Sigma-Aldrich. Potassium carbonate (K_2CO_3, 124785, 99.995% trace metals basis – Lot 50006293) was purchased from BeanTown Chemical. Nitrile examination gloves (82026-426) and Corning® centrifuge tubes (430828 & 430790, 50 mL and 15 mL, respectively) were purchased from VWR International. 400 grit sandpaper (Norton Blue Bak, waterproof) and 1500 grit sandpaper (G2, waterproof, Finish 1st) were purchased from W.W. Grainger Inc. Aluminum foil used as a current collector for the electrochemical cell and as a surface on which to polish the catalyst foil was commercially available Reynolds Wrap.

S.2 Cell Design

A two-compartment cell was used for all electrochemical experiments discussed in this text.[1] This cell was manufactured out of polycarbonate by Lab Machinist Solutions. Plugs and connections that served as the cell parts were made of polypropylene, while ferrules were made of ETFE (Tefzel™); these parts were purchased from IDEX Health & Science. O-rings to seal the compartments upon assembly were made of FEP-Encapsulated Silicone (9319K15 & 9319K142) and were purchased from McMaster-Carr. The design of the openings for the catalysts in the cell was such that 1 cm^2 would be exposed to electrolyte. In this way, partial currents obtained in electrochemical experiments were converted directly to partial current densities.

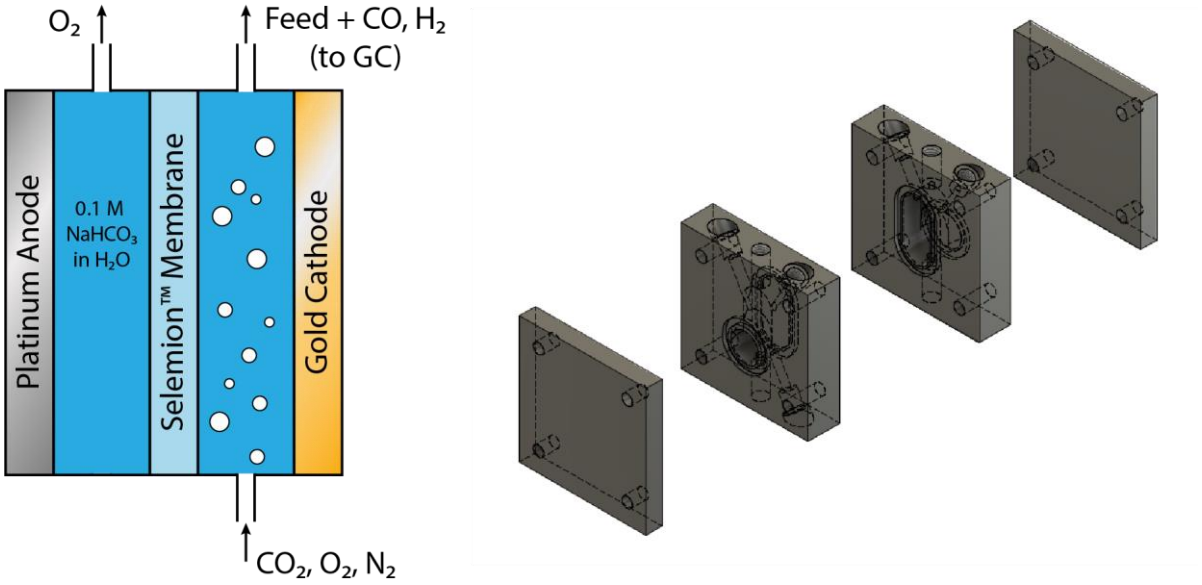

Figure S1. Schematic of the electrochemical cell and flow scheme used in these experiments.[1]

S.3 Electrolyte preparation

Sodium bicarbonate electrolyte was prepared by dissolving enough sodium carbonate in Milli-Q® to yield sodium carbonate of half of the desired final bicarbonate molarity. For example, in preparing 200 mL of 0.1 M sodium bicarbonate, 1.06 g of Na_2CO_3 was dissolved in 200 mL of water to yield 0.05 M sodium carbonate. This solution was then bubbled overnight (using 1/16" tubing submerged in the electrolyte solution) to convert the carbonate to bicarbonate using Instrument grade CO_2. Electrolyte solutions were stored in colorless polypropylene containers (VWR). They were bubbled periodically as used, with a bubbling time of 30-60 minutes sometime within the day before use in an experiment.

S.4 Foil preparation

Au foils were prepared by placing the 25x25 mm catalyst foil on a clean aluminum foil polishing surface, then covering the face of the Au foil with roughly 1 mL Milli-Q® water, and subsequently hand-polishing (while wearing fresh nitrile gloves) with 400 grit sandpaper for 3 minutes. Foils were scrubbed gently but thoroughly, moving in a circular pattern and rotating the foil throughout the polish. A few mL of fresh Milli-Q® were used to gently rinse the surface of the foil. The foil was then submerged in Milli-Q® within a 50 mL centrifuge tube and sonicated for 3-5 minutes. VEVOR PS-10A (2 L; 60 W, 40 kHz) Ultrasonic Cleaners were used interchangeably with a VWR Symphony™ (97043-992; 90 W, 35 kHz) Ultrasonic Cleaner for this purpose. The Milli-Q® was then decanted, and the foil dried off by passing it under a stream of house-supplied compressed air.

Foils were designated as having a "back" and a "front," so that only one side of the foil was polished and used in catalysis throughout the foil lifetime.

S.5 Reference Electrode Calibration

3.4 M Ag/AgCl reference electrodes used in the experiments were calibrated in the morning before each experiment in order to prevent reference potential drift. These leak-free references were stored with their frits submerged in vials of Milli-Q® water. The reference electrode to be calibrated was placed in a solution of saturated KCl (i.e. a solution of Milli-Q® at equilibrium with solid KCl in the bottom of the vial) along with a saturated master electrode. The master electrode was purchased with 1.0 M KCl filling, but was stored in an insulation-wrapped vial of saturated KCl in Milli-Q® and not used in any electrochemical experiments. Because the master electrode had a porous frit which allowed ion transport, storing the electrode in saturated KCl caused it to take on the characteristics of a saturated KCl reference. The Ag/AgCl in saturated KCl master reference was then taken to be +0.197 V vs. SHE.[2] By hooking up the master as the counter/reference electrode and the experimental reference as the working electrode using a BioLogic VMP3 potentiostat, it was possible to monitor (either through observation or data-recorded OCV experiments) the potential difference between the two references in the same saturated KCl solution. In this way, the reference electrode values were adjusted daily. For instance, a morning reading indicating the experimental reference was +0.016 V vs. the master was interpreted to mean the experimental reference was +0.213 V vs. SHE on that day. Long-term data collection suggests that the reference most used in this work drifted upwards by less than 1 mV (0.001 V) per day – roughly 25 mV per month – through constant storage in Milli-Q® water.

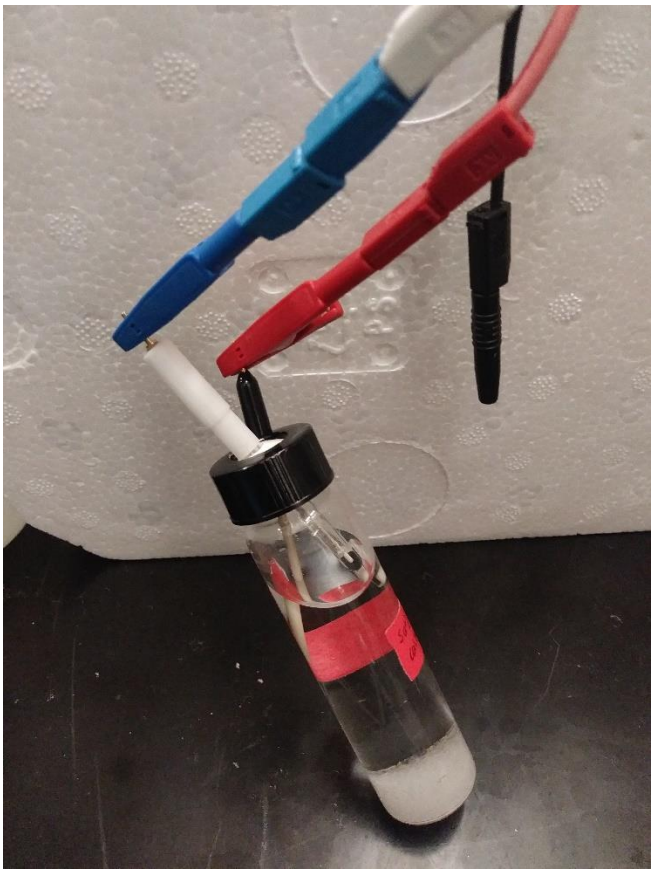

Figure S2. Calbrating the LF-2 Ag/AgCl reference electrode used in experiments to a master saturated Ag/AgCl reference.

Conversion between voltages applied on an SHE scale and an RHE scale:

$$U_{RHE} = U_{SHE} + 0.059pH$$

The bulk pH value of 0.1 M bicarbonate is taken to be 6.8 at 1 atm CO_2 and 7.1 at 0.5 atm CO_2, and the broadly-used conversion in this work is that 0 V vs. RHE corresponds to -0.41 V vs. SHE.

S.6 Gas Mixing and Flow Scheme

A three-gas mixing setup was constructed using three flow controllers (MC-50SCCM-D/5M, 5IN, GAS: Air; accurate to two decimal places in sccm) purchased from Alicat Scientific. One was hooked up to CO_2 via lab manifold dropdown lines and 1/8" FEP tubing (Cole-Parmer, EW-06406). Another controller was connected to house N_2 through 1/8" FEP tubing. These two gases were mixed using an ETFE (Tefzel™) tee from IDEX Health & Science. The resulting stream was

carried off the center connection of the tee and through an additional 1/8” FEP tubing section, then united with a gas line coming off of a free-standing oxygen tank through 1/8” FEP. This combined stream from all three gas sources was conveyed by another section of 1/8” FEP and then bubbled through a 20-mL hydration bubbler (maintained between 1/3 and 2/3 full with Milli-Q® water). This stream was sent into the electrochemical setup using a 1/16” FEP tubing. A 1/16” tubing section exiting the electrochemical setup then conveyed gas to a mostly-empty 20 mL vial where it was mixed in order to average out any bubbles of evolved gas leaving the electrochemical cell. 1/8” FEP tubing connected the outlet of this mixing vial to an Alicat flow meter (MS-100SCCM-D/5M, GAS: Air; accurate to 1 decimal place in sccm). This flow meter helped to ensure there were no gas leaks anywhere in the flow configuration. The outlet of this flow meter was sent to a gas chromatograph (SRI Instruments, Inc., Model 8610C) where gas products were detected in-line. The sample loop vented to local exhaust when samples were not being loaded onto the GC columns; when samples were injected, the analyzed products were vented to the ambient environment in an intrinsically safe fashion (the last analytical device in the gas line was an FID, which converted all hydrocarbons and hydrogen to CO_2 and water). Disjointed tubing sections throughout the gas flow setup were connected by ETFE (Tefzel™) unions (IDEX Health & Science).

Custom gas mixes were programmed into the Alicat flow controllers and meter to ensure proper flow rates and closures. An example of such a mixture includes 50% CO_2, 37.5% N_2, 12.5% O_2.

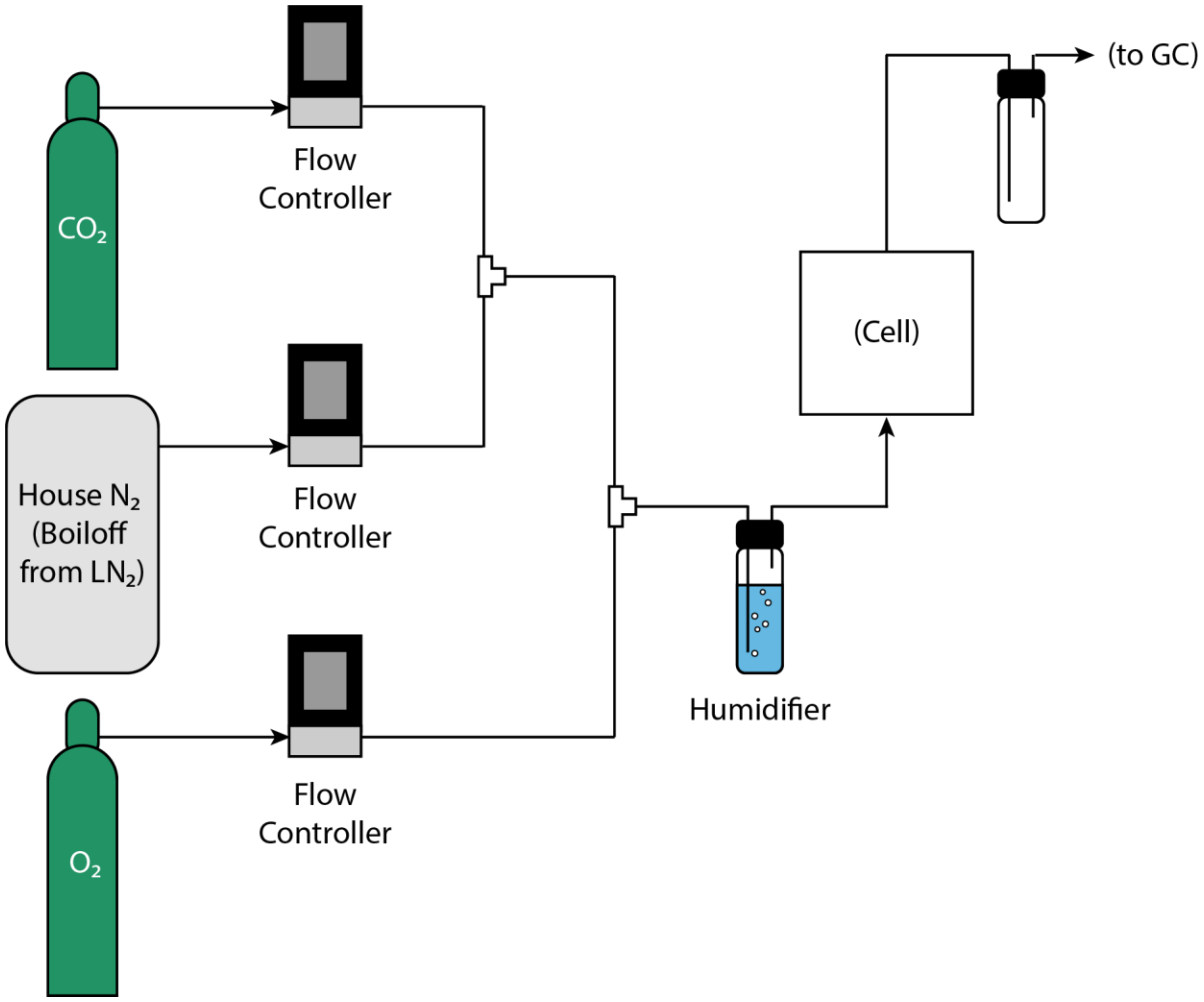

Figure S3. Schematic for gas flow through the system.

S.7 Electrochemical Experiments

In preparation for an electrochemical experiment, the polycarbonate cell and all cell parts in immediate contact with the electrolyte (plugs for working compartment; reference electrode connector & ferrule; plug for counter compartment) were submerged in 20% v/v nitric acid. The polycarbonate (PC) was removed from nitric acid after less than one minute so as to avoid PC dissolution or etching (as PC is not compatible with nitric acid over long exposure times). The PC cell (with o-rings assembled) was then rinsed with Milli-Q® and allowed to air-dry. The 20% nitric acid was decanted off of the cell parts after roughly five minutes, and the parts were triple-rinsed with Milli-Q®. These parts were placed onto a clean absorbent towel (WypAll Cleaning Wipes) and allowed to air-dry. The Au foil was then polished and prepared according to the procedure described above. The Pt counter-electrode was placed on the aluminum current collector for the anode side, then the counter compartment was used to sandwich the foil in place. A new piece of Selemion™ (stored in Milli-Q®; roughly 2 cm by 4 cm; enough to cover the window between the

two cell compartments) was then cut using scissors which were reserved for cutting membranes and dried after each use. The Selemion™ was rinsed with fresh Milli-Q® and assembled into the cell, followed by the working compartment, then the gold foil. Once the second backplate of the cell was in place, the pieces were bolted together with wing nuts and tightened with a hex key. A calibrated reference electrode was then inserted into the reference port of the working electrode compartment of the cell using an extra-long IDEX connector and a 2.0 mm ferrule. The bottom port of the working side of the cell was then connected to the gas mixing setup, with the desired flow of each component already set; meanwhile, the bottom port of the counter compartment was plugged with a polypropylene plug. Flow rates for the gases were modulated depending on the type of experiment being conducted. Unless otherwise indicated, all experiments were conducted with a total inlet gas flow rate of 10 sccm. (So a normal gas flow consisting of 0.5 atm CO_2 and 0.5 atm O_2 would be fed as 5 sccm CO_2, 5 sccm O_2.)

The prepared electrolyte was loaded into the cell using the same plastic pipette tip for each test. 1.75 mL was used to fill each side of the cell. After filling, the working compartment of the cell was then closed from the atmosphere by plugging the top ports on the cell diagonals, and the center port was hooked up to the gas flow system as described above. The cell was then allowed to sit while bubbling for roughly 15 minutes to allow air to flush out of the gas flow lines. Meanwhile, the reference and anode/cathode current collectors were hooked up to a BioLogic VMP3 potentiostat. Upon beginning an experiment, a blank GC sample was initiated; GC samples were taken every 10 minutes thereafter, with the results at t = 10 minutes thrown out due to lack of complete mixing. To compute faradaic efficiencies and partial current densities, the data points at t = 20, 30, and 40 minutes were averaged. Long-time experiments were avoided due to persistent current decay over time during electrochemical reduction on gold (consistent with previous literature observations; see Section S.10).

IR compensation was handled in each experiment by performing potentiostatic electrochemical impedance spectroscopy (PEIS – frequency range 10 kHz-1 Hz) and visually extrapolating the EIS curve to the x-intercept (estimating to the nearest Ohm). 85% IR compensation was then applied. Typical 100% IR compensation values obtained from PEIS were 70 Ohms for 0.1 M $NaHCO_3$ and 5-15 Ohms for 1.0 M sodium electrolytes.

All data points were gathered independently of one another and in a randomized order to ensure no bias by variables drifting in time. That is, a new cell was prepared as described above for each data point reported herein.

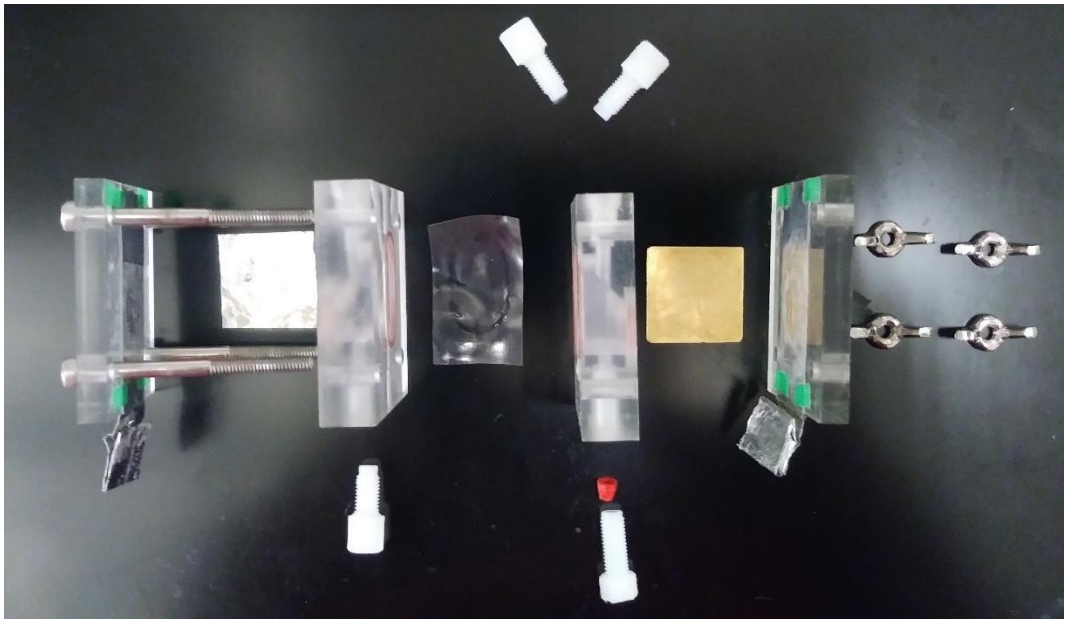

Figure S4. Image of disassembled electrochemical cell, including (L-R): Backplate with bolts and Al foil current collector, Pt counter electrode, counter electrode compartment, plug, Selemion membrane, working electrode compartment, plugs and reference electrode adapter, Au working electrode, backplate with Al foil current collector, and wing nuts.

Steps in cell construction:

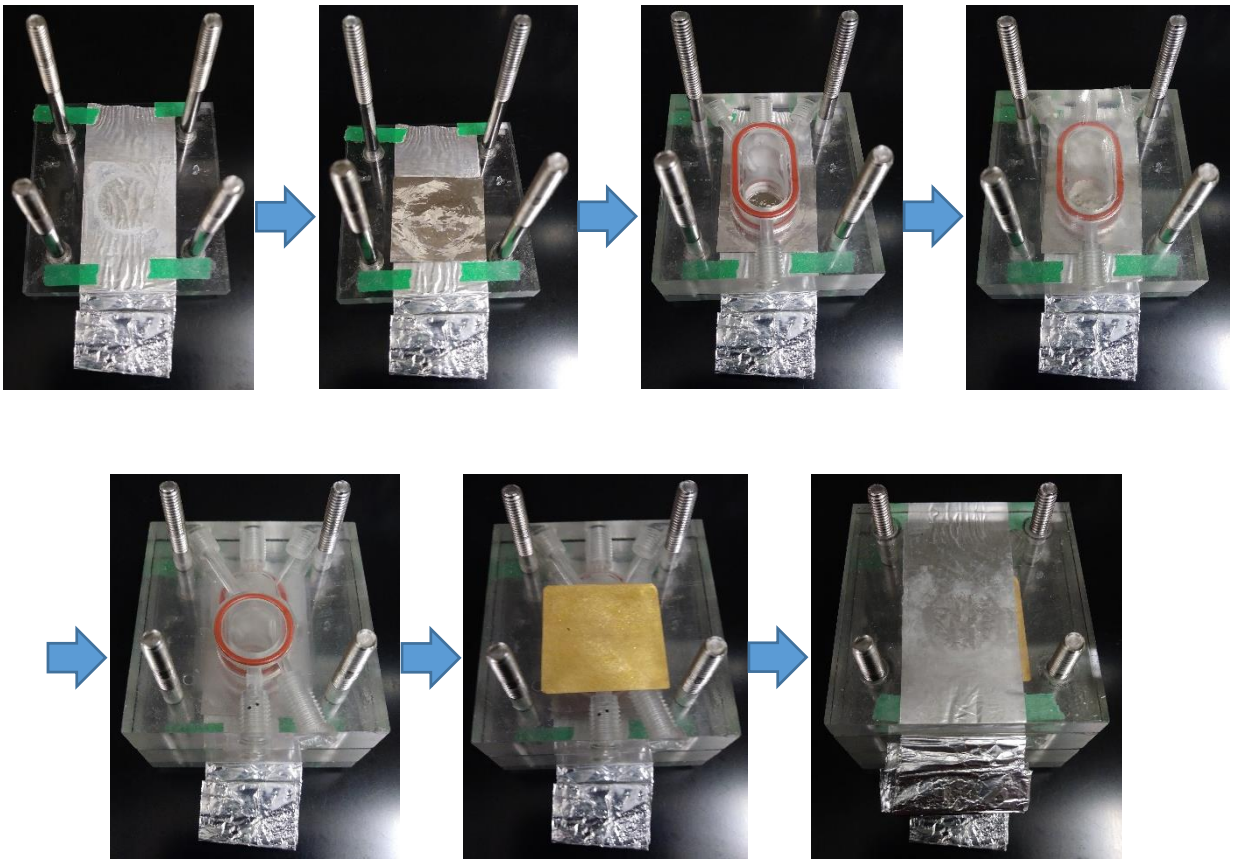

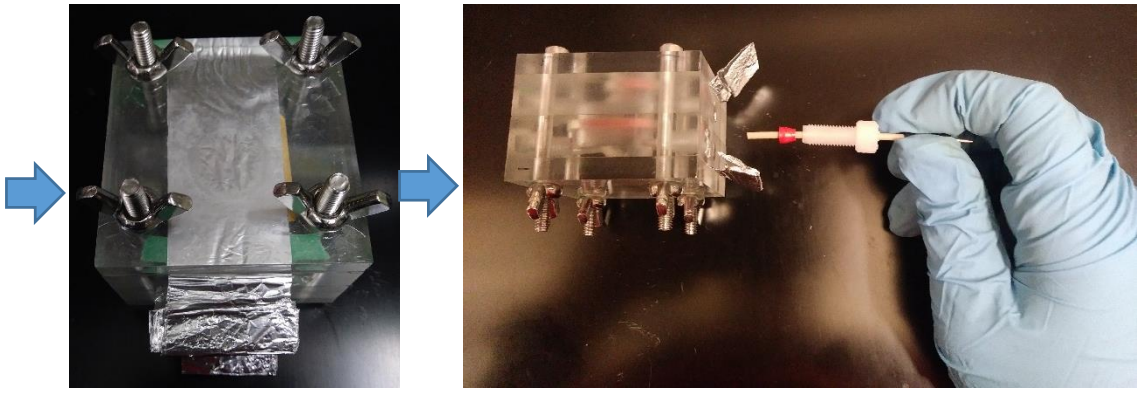

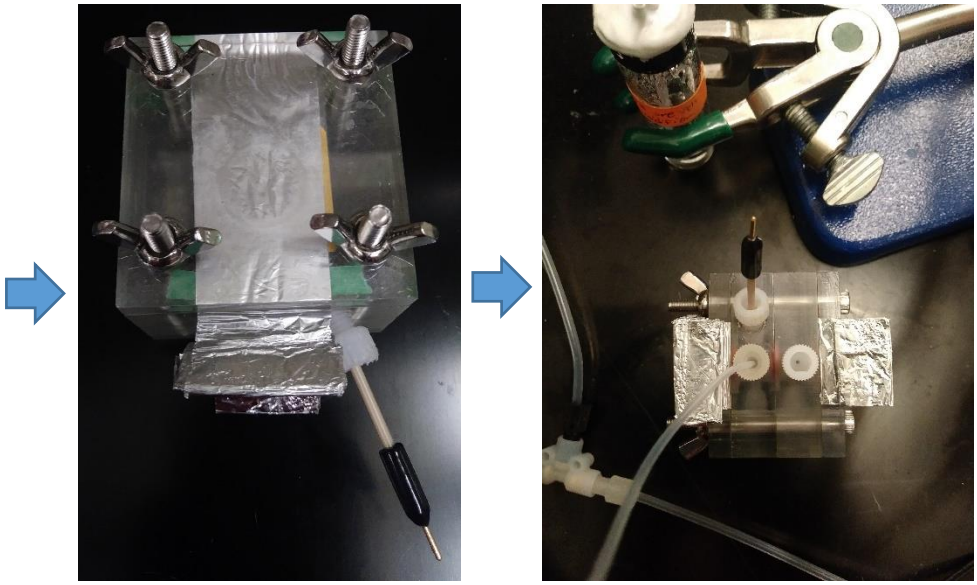

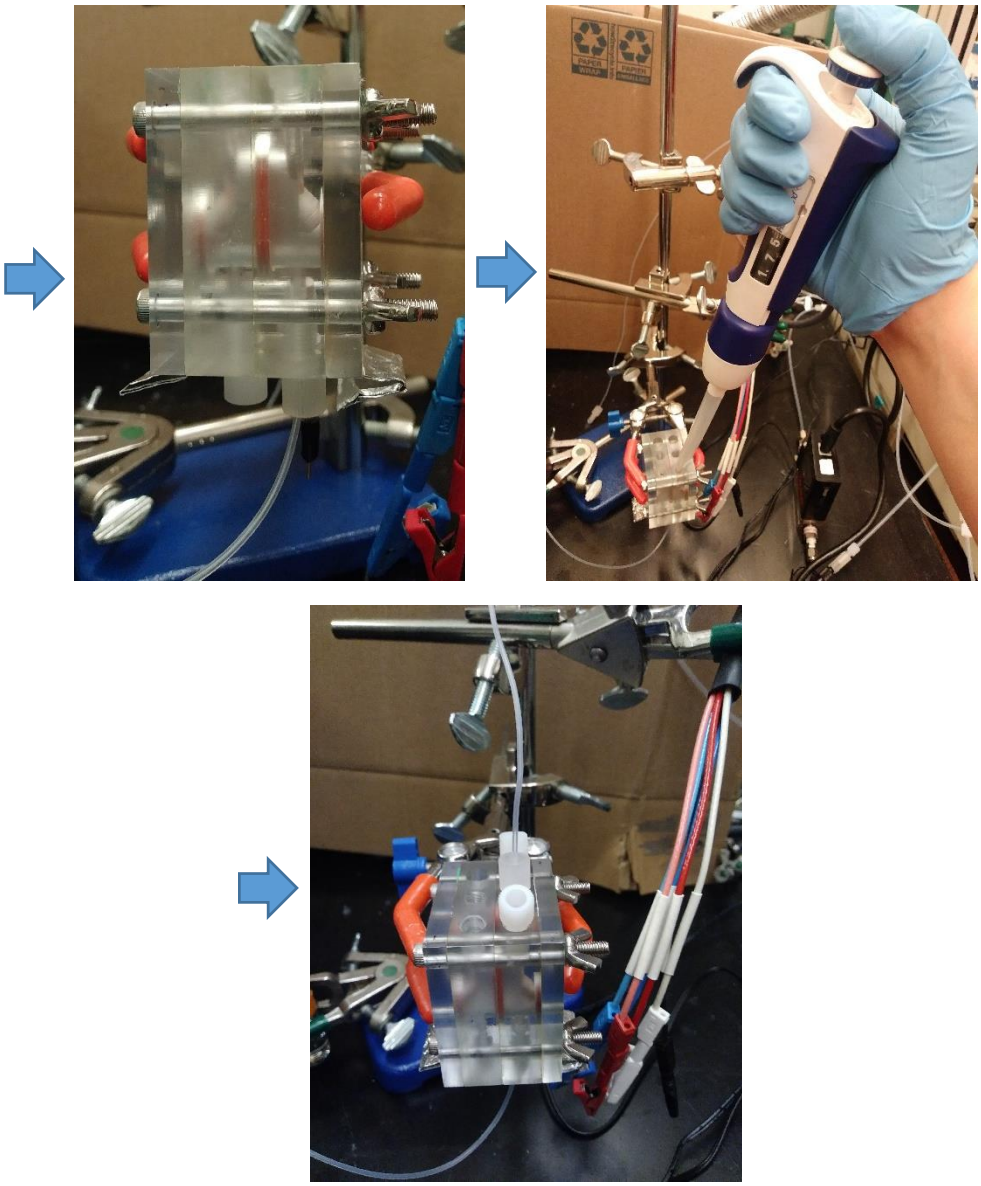

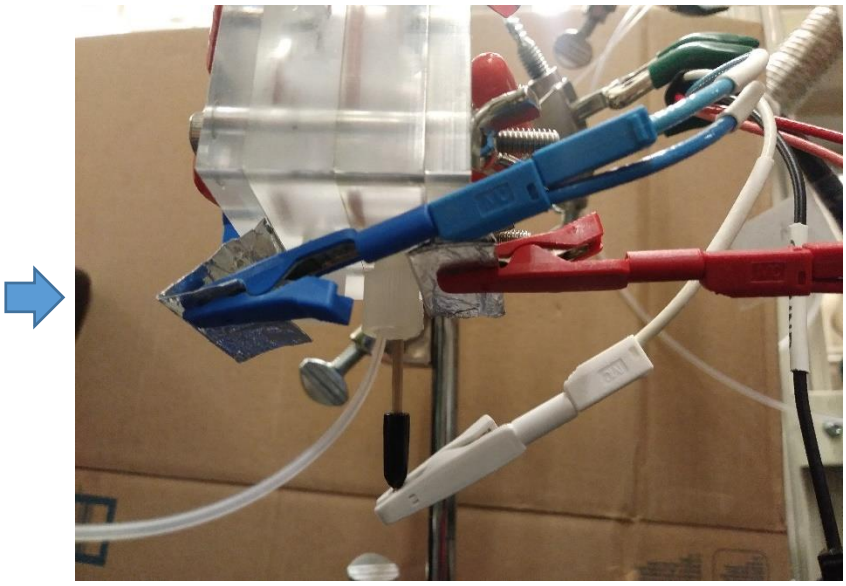

Figure S5. Steps in cell construction, from laying down the Pt electrode to connecting the closed cell to potentiostat cables.

S.7.1 P_{O2} Effect, Tafel Analysis, and CO_2 Order Dependence Studies

P_{O2} effect and Tafel analysis data points were gathered as described above. P_{O2} effect was determined by holding CO_2 flow rate constant at 5.00 sccm and varying O_2 pressure (through flow rate), while using N_2 to balance the total flow to 10.00 sccm. Tafel analysis was conducted with either 5.00 sccm CO_2/5.00 sccm N_2 or 5.00 sccm CO_2/5.00 sccm O_2 and varying the applied potential. CO_2 order dependence was determined by holding oxygen flow rate constant at either 0.00 sccm or 5.00 sccm and varying CO_2 pressure (through flow rate), while using N_2 to balance the total flow to 10.00 sccm.

S.7.2 Bicarbonate Order Dependence Studies

Bicarbonate dependence was probed by holding absolute potential constant (vs. SHE) – not potential vs. RHE. This is for reasons discussed below. Bicarbonate concentration was varied while holding total solution ionic strength constant. This was done using sodium perchlorate as the supporting electrolyte. In most cases, the electrolyte was made by mixing prepared 1.0 M sodium bicarbonate (made using ≥99.0% pure untreated sodium carbonate, Sigma-Aldrich S7795, Lot SLBT0414) with 1.0 M sodium perchlorate in the desired ratio. For instance, 0.4 M bicarbonate solution was made by mixing 4 mL of 1.0 M bicarbonate with 6 mL of 1.0 M perchlorate. For the potassium bicarbonate order dependence experiments detailed in the SI, it was

not possible to balance the electrolyte with perchlorate, as potassium perchlorate is not soluble up to 1.0 M. Thus, these experiments were conducted at different total ionic strengths.

In interpreting these experiments, data was normalized by the concentration of CO_2 in solution, as the solubility variable changes slightly with different electrolyte compositions. The relationship describing CO_2 solubility in a multi-component salt solution is described reasonably well by:[3]

$$\log\left(\frac{c_{G,0}}{c_G}\right) = \sum_i (h_i + h_G)c_i$$

where $c_{G,0}$ and c_G represent gas solubility in pure water and the salt solution, respectively, and c_i is the molar concentration of the ion *i* in solution. This is an empirical fit with experimental validity up to roughly 2 M. The coefficients h_i and h_G given in this reference for Na^+, HCO_3^-, ClO_4^-, and CO_2 yield the following result at room temperature:

$$\log\left(\frac{c_{CO_2,0}}{c_{CO_2}}\right) = (0.1143 - 0.0172)c_{Na} + (0.0967 - 0.0172)c_{HCO_3} + (0.0492 - 0.0172)c_{ClO_4}$$

Since the solubility of CO_2 in pure water at room temperature and pressure is 34 mM,[4] we obtain the following for a half atmosphere of CO_2 (solubility 17 mM):

$$\log\left(\frac{17\ mM}{c_{CO_2}}\right) = 0.0971c_{Na} + 0.0795c_{HCO_3} + 0.0320c_{ClO_4}$$

In the case where we hold the ionic strength constant at 1.0 M, we can substitute the following expressions for c_{Na} and c_{ClO4}:

$$c_{Na} = 1, \qquad c_{ClO_4} = 1 - c_{HCO_3}$$

Then by rearranging the logarithmic expression above, we obtain the following for the concentration of CO_2:

$$c_{CO_2} = [17\ mM] \cdot 10^{0.1291 - 0.0475 c_{HCO_3}}$$

S.7.2.1 Sodium Bicarbonate Experiments at High Bicarbonate Concentration

Sodium bicarbonate experiments were carried out at up to 1.0 M $NaHCO_3$, but at very high concentrations, extremely low currents to both CO_2RR and HER were observed (**Figure S6**). It is estimated that this is due to a secondary effect such as metal impurity plating or being close to the solubility limit of bicarbonate.

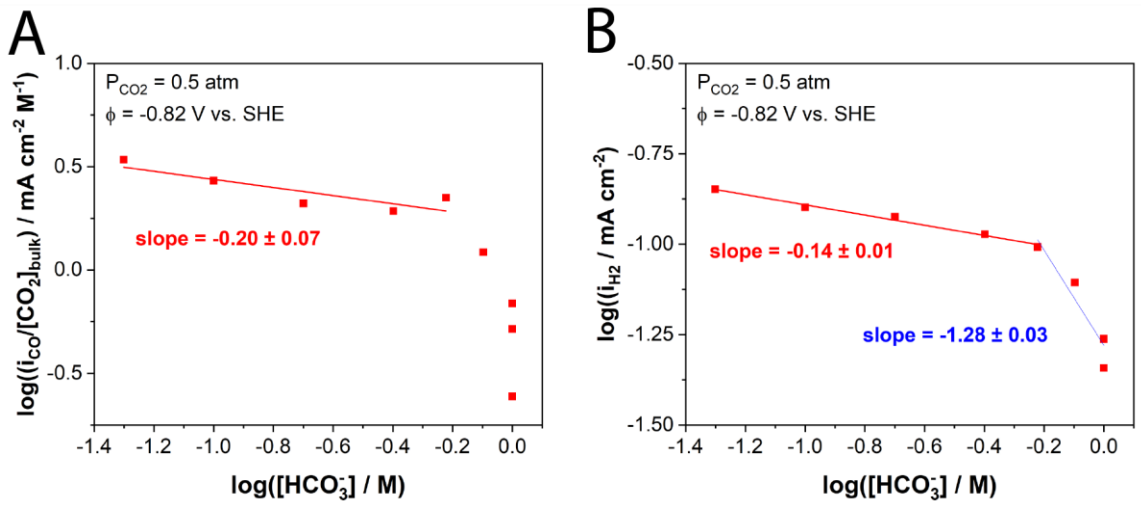

Figure S6. Bicarbonate dependence of both (A) CO_2RR and (B) HER at a wide range of bicarbonate concentrations.

S.7.2.2 Potassium Bicarbonate Experiments

Bicarbonate order dependence was studied with unbalanced potassium bicarbonate electrolyte, resulting in the conclusion that the negative dependence of CO_2RR on sodium bicarbonate was due to some secondary effect. Note in the case of $KHCO_3$ that there appears to be a region in which there is a positive dependence upon bicarbonate, but that this is below the concentrations at which the experiments employed in this work operate.

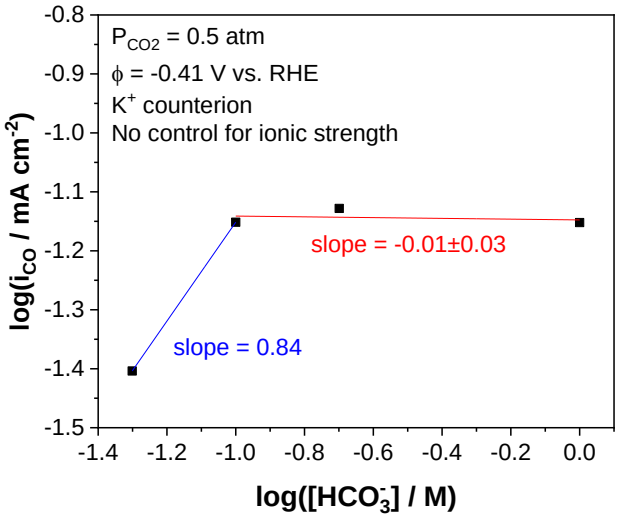

Figure S7. Bicarbonate order dependence using potassium bicarbonate as the electrolyte.

S.7.3 KIE Experiments

The kinetic isotope effect was elucidated by preparing electrolyte in the same way as other experiments, but this time using D_2O. D_2O was removed from its sealed container with a syringe. Special care was taken when bubbling the D_2O-based electrolyte to cover the top of the container it was in, in order to prevent absorption of H_2O in the air. Other changes to procedure relative to the standard CO_2 reduction were:

- Cell drying: rather than allowing cell and cell parts to dry in air, all parts were dried in an 80 °C oven for at least 15-20 minutes to evaporate as much residual water as possible.
- Selemion™ soaking: prior to use in the experiment, the Selemion™ membrane to be used in the experiment was shaken dry, placed in a nitric-acid-cleaned petri dish (no more than 5 cm in diameter), and covered in a thin layer (~4 mL) of D_2O. The dish was covered to prevent atmospheric water uptake, and the membrane was allowed to soak for roughly half an hour. After this time had elapsed, two more 4 mL soaks were provided, each with soak times on the order of 10 minutes. This helped to prevent adventitious water sources that may have convoluted the results of the experiment.
- Hydration bubbler: switched out the normal water hydration bubbler to a D_2O-based bubbler.

For HER quantification in the deuterated solvent case, it was necessary to perform normalizations on the raw H_2 data, as the thermal conductivity detector used in product detection was less sensitive to D_2 than to H_2. It was gathered from existing literature that the sensitivity factor (ratio of D_2 peak to H_2 peak area of identical concentration) should be roughly 0.75,[5] but this was tested for our instrument by preparing a conductive electrolyte without CO_2 (0.1 M $NaClO_4$ in D_2O) and bubbling N_2 through the solution at 10 sccm to remove any dissolved O_2 and/or CO_2, then applying a constant current of -0.5 mA to the system and quantifying the hydrogen signal as a result of HER. From this, it was found that the appropriate sensitivity factor was 0.7031, so a conversion factor corresponding to the reciprocal of this value – 1.4223 – was applied to all hydrogen signals for experiments with deuterated electrolyte.

S.7.4 Modified Cyclic Voltammetry

Cyclic voltammetry, modified to study characteristics of the non-quiescent cell, was used as evidence that the onset of ORR occurred at a much less reductive potential than required for CO_2RR or HER in the system in question – and, moreover, that ORR was transport-limited at the tested voltages. CVs were conducted in 0.1 M $NaHCO_3$, and were IR-corrected just as constant-potential experiments were. The CV blank was obtained by bubbling N_2 at 10 sccm and scanning from +1.00 V vs. SHE to -0.40 V vs. SHE and back, while the CV with O_2 and CO_2 was obtained

by scanning from +1.00 V vs. SHE to -0.80 V vs. SHE and back (this extends the first test to within the Tafel regime and after CO_2RR/HER onset).

While the main-text scan (Figure 2A) does not highlight this feature, a persistent observation during these experiments was an initial reductive wave around 0.2 V vs. SHE, followed by another reduction which quickly became transport-limited around -0.2 V vs. SHE. This is highlighted more clearly in the figure below. We hypothesize that the initial reductive wave is the more kinetically facile ORR to peroxide, while ORR to water takes over when overpotentials and current densities are higher.

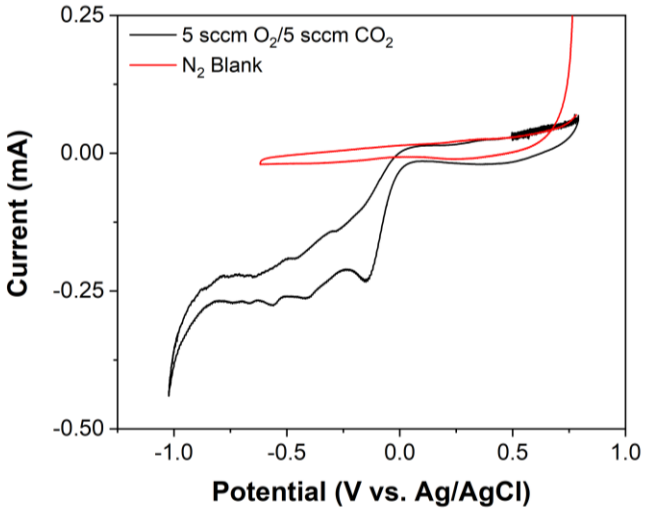

Figure S8. Modified cyclic voltammogram better highlighting the different reductive waves observed during ORR onset.

S.7.5 Measuring Boundary Layer Thickness

Because transport is so integral to dictating oxygen's effect on the CO_2RR system, it was useful to quantify the boundary layer thickness at the surface of the cathode in the cell. This was done using a procedure from Clark et al.[6] A full description may be found in the cited work's Supporting Information, section SI-4.

In short, mass transport boundary layer thickness was quantified by measuring the diffusion-limited current of a known reaction – ferricyanide reduction to ferrocyanide:

$$Fe(CN)_6^{3-} + e^- \rightarrow Fe(CN)_6^{4-}$$

Two bicarbonate solutions were made – one 0.1 M in $NaHCO_3$, and the other 1.0 M in $NaHCO_3$ – and both of these were made to be 0.01 M in $K_3Fe(CN)_6$ by addition of 32.9 mg ferricyanide salt per 10 mL electrolyte solution. By performing a CV extending from roughly +1.1 V vs. RHE (+0.69 V vs. SHE) to -0.4 V vs. RHE (-0.81 V vs. SHE) in the 0.1 M solution, it was possible to extract the mass transport boundary layer thickness from the steady-state current density at the

plateau of the CV. This plateau occurs from roughly +0.5 V vs. RHE to -0.2 V vs. RHE. Taking the value at around +0.1 V vs. RHE to be a good middle point, the steady-state current density can be related to boundary layer thickness by:

$$\delta_{BL} = \frac{F \cdot D_{Fe(CN)_6^{3-}} \cdot C^*_{Fe(CN)_6^{3-}}}{i_{SS}}$$

where F is Faraday's constant, $D_{Fe(CN)_6^{3-}}$ is the diffusivity of the ferricyanide ion (this is taken to be 0.720×10^{-5} cm^2 s^{-1}),[7] $C^*_{Fe(CN)_6^{3-}}$ is the concentration of ferricyanide ion in the bulk of the electrolyte, and i_{SS} is the steady-state current.

It should be noted that the accuracy of the boundary layer thickness when determined this way is contingent upon migration being negligible. The ferricyanide ion in these tests is dilute enough in the supporting salt that migration effects can be ignored; and moreover, experimental evidence suggests no substantial difference between reduction currents under the above protocol for 0.1 M and 1.0 M bicarbonate electrolytes.

Using this method, the δ for ferricyanide mass transport was found to be 140 μm, as the steady-state reduction current density was around 0.497 mA cm^{-2}.

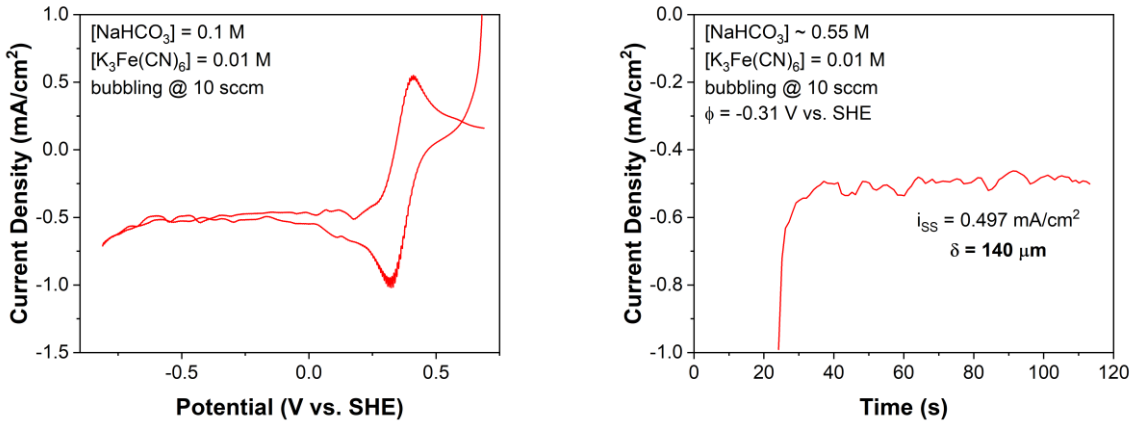

Figure S9. CV to identify the proper potential for testing boundary layer thickness, and CA to determine limiting current density of ferricyanide reduction.

S.7.5.1 Conversion of ferricyanide boundary layer to relevant species' boundary layer

The delta obtained above is the accurate value for the transport of the ferricyanide ion; however, an adjustment must be applied in order to obtain δ_j for the dissolved gas species.

It can be (and has been) derived that the concentration boundary layer δ_C and momentum boundary layer δ_M scale as such:[8]

$$\delta_C \sim Re^{-1/2} Sc^{-1/3}$$

$$\delta_M \sim Re^{-1/2}$$

So that, for reference,

$$\frac{\delta_M}{\delta_C} \sim Sc^{1/3} = \left(\frac{\nu}{D}\right)^{1/3} \gg 1$$

Or, because the Schmidt number *Sc* to the 1/3 power is much greater than 1 for almost all liquids, including water, the concentration (or mass-transport) boundary layer δ_C is embedded within the momentum boundary layer δ_M. To understand the nature of how different species' mass transport boundary layers scale with one another, we expand the expression for δ_C, where below the δs correspond to the concentration boundary layers for the subscripted species:

$$\delta_j \sim Re^{-1/2} Sc^{-1/3} = \left(\frac{uL}{\nu}\right)^{-\frac{1}{2}} \left(\frac{\nu}{D_j}\right)^{-1/3}$$

So that the following is true:

$$\frac{\delta_{Fe(CN)_6^{3-}}}{D_{Fe(CN)_6^{3-}}^{1/3}} = \frac{\delta_{CO_2}}{D_{CO_2}^{1/3}} = \frac{\delta_{O_2}}{D_{O_2}^{1/3}}$$

Rearranging to find the boundary layer thickness for either of the gas-phase species, we obtain:

$$\delta_{gas} = \delta_{Fe(CN)_6^{3-}} \left(\frac{D_{gas}}{D_{Fe(CN)_6^{3-}}}\right)^{1/3}$$

The diffusion coefficient of ferricyanide is as above taken to be 0.720×10^{-5} cm^2 s^{-1}.[7] Diffusion coefficients for CO_2 and O_2 are taken as 1.92×10^{-5} cm^2 s^{-1} and 2.10×10^{-5} cm^2 s^{-1} respectively.[9] Therefore, the conversion factor from the above ferricyanide boundary layer of 140 μm is 1.387 in the case of CO_2 and 1.429 in the case of O_2, making the values of boundary layer thickness:

$$\boldsymbol{\delta_{CO_2} = 194\ \mu m, \quad \delta_{O_2} = 200\ \mu m}$$

Further, noise in the current signal during the chronoamperometric experiment in S.7.5 can be used to put errors on these values; in the case of the signal pictured above, the final value for the boundary layer thickness for O_2 is 200±7 μm.

This value is larger than the reported ferricyanide boundary layer thickness for similar cells in the literature, which report $\delta_{Fe(CN)_6^{3-}} \approx 50$ μm at gas bubbling = 10 sccm;[6] however, differences in gas bubbling techniques in the cells may account for this difference.

S.8 Product Detection

The product of CO_2 reduction on gold is typically CO. CO_2 can, however, be reduced further to methane, ethylene, and even liquid products such as short-chain alcohols. The competing reaction, HER, generates H_2. Oxygen reduction on gold generates water or peroxide, depending on the pH and other cell conditions. It was necessary to quantify the various reactions occurring during the electrochemical reduction experiments. This was done primarily through in-line gas chromatography, but the results are also supported by negative results of product detection through both liquid ^{1}H-NMR and a UV-visible quantification method for determining peroxide concentration.

It should be noted that, for all experiments implementing O_2, the ORR current was interpreted from the lack of Faradaic closure, as water produced during ORR could not be quantified.

S.8.1 Gas Chromatography

An in-line gas chromatograph (SRI Instruments, Inc., MG #5, Model 8610C) with auto-sampling capabilities was used for gas-phase product detection. N_2 gas available in-house was used as the GC carrier gas, and was adjusted to roughly 16.5 psig on the instrument. Data sample rate was 5 Hz. The GC was calibrated to detect CO and H_2, although representative tests on other instruments also allowed for confirmation that the products CH_4, C_2H_4, and C_2H_6 were not produced during CO_2 reduction on gold.

Gas flow into the GC was normally vented out through a 1-mL sample loop. The GC configuration was modified so that upon sample injection, gas flow was sent onto a 6’ HayesepD pre-column. After this pre-column, gas flowed onto a 6’ MS-5A column. Finally, gas was analyzed with both a thermal conductivity detector (TCD) and a flame ionization detector (FID; coupled with a methanizer to detect products such as CO). Burnt sample gas was vented to ambient air as CO_2 and water.

The long pre-column allowed for adequate column elution times so that hydrogen and oxygen could be resolved, while at the same time excluding components from the MS-5A such as CO_2, water, and hydrocarbons heavier than methane. These heavier components cannot be separated on an MS-5A column, and therefore were excluded from loading by backflushing the pre-column around the pre-column elution time for methane. The order of elution from the pre-column was: Hydrogen – Oxygen – CO – Methane – CO_2 – Ethylene – Ethane – Water. The order of elution out of the entire system was: Hydrogen – Oxygen – Methane – CO. Note that while CO emerges from a HayesepD column before methane, it elutes later than methane on an MS-5A. The species spend a longer time on the MS-5A, so the elution of CO and CH_4 out of the entire system is swapped relative to coming out of the pre-column.

GC Event Sequence:

Time (min)	Event
0.000	Zero baseline
0.050	G valve on (Flow forward through HayesepD pre-column)
2.600	G valve off (Flow backward through HayesepD pre-column)
5.250-6.600	Integration-based baseline adjustments
8.000	Program ends; wait at least 2 minutes to cool all the way back down to 50 °C before loading next sample

GC Temperature Profile:

50 °C for 2.6 minutes, 0.9 minute ramp to 170 °C, 2 minute hold at 170 °C, 2.9 minute ramp down to 50 °C.

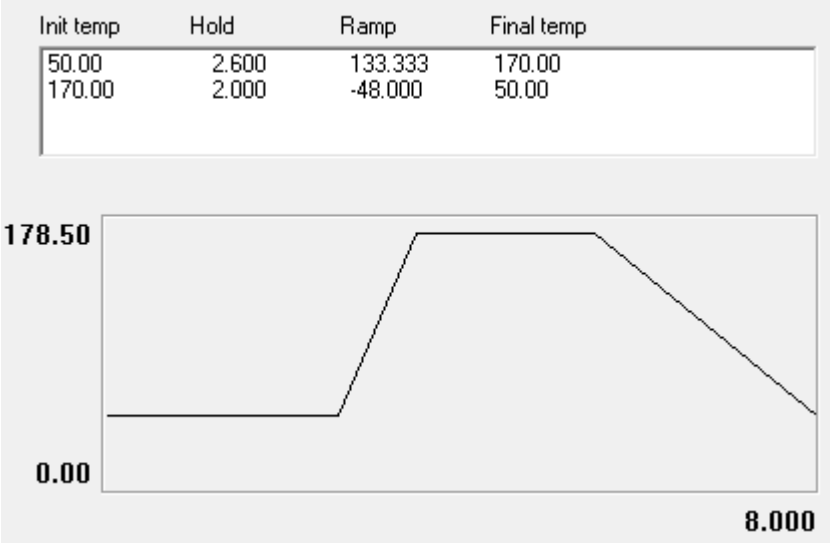

The GC was calibrated using two standard gas solutions, representing low- and high-concentration samples.

Concentrations in ppm of gases in the calibration gas tanks.

Gas	H_2	O_2	CO	CH_4	C_2H_4	C_2H_6
1,000 ppm Cal. Gas	980	990	990	990	980	980
10,000 ppm Cal. Gas	10,000	0	10,000	10,200	0	0

The pure CO_2 tank contained < 0.554 ppm of CO (per Airgas specifications) and negligible amounts of other gases, so it was assumed to be pure CO_2. Calibration gases both had CO_2 as the balance.

To calibrate, GC samples were taken every 10 minutes (8-minute program, 2 minutes to purge sample loop of carrier gas and cool down). One 20 mL hydration mixing vial (half filled) and one 20 mL empty vial were used prior to insertion into the GC. No baseline subtraction was used.

An Alicat FlowVision script was written to automatically change gas flow rate set points every 4 samples (40 minutes), starting 60 seconds after the last sample at a given concentration was injected. See the table below for flow controller settings.

1,000 ppm Cal. Gas (sccm)	Pure CO_2 (sccm)	Nominal ppm Value	File Numbers
High FID Sensitivity			
20	0	1000	1-5
18	2	900	6-9
10	10	500	10-13
6	14	300	14-17
2	18	100	18-21
1	19	50	22-25
0.5	19.5	25	26-29
0.5	30	16.4	30-33
0.5	40	12.3	34-37
0.3	40	7.4	38-41
Medium FID Sensitivity			
2	18	100	42-46
10	10	500	47-50
20	0	1000	51-54
10,000 ppm Cal. Gas (sccm)	Pure CO_2 (sccm)	Nominal ppm value	File Numbers
High FID Sensitivity			
0.5	19.5	250	55-59
2	18	1000	60-63
3	17	1500	64-67
3.8	16.2	1900	68-71
Medium FID Sensitivity			
0.5	19.5	250	72-76
2	18	1000	77-80
6	14	3000	81-84
10	10	5000	85-88
14	6	7000	89-92

Chromatogram processing: no baseline subtraction or smoothing was conducted, nor were the windows of integration around the components shifted. Data are given as-collected from the above experiments.

Calibration Curve Results:

Area Calibration Parameters for FID High Signal

Gas	Retention Time (min)	m	b	σ_m^2	σ_b^2	σ_{mb}^2	RMSE (ppm)	R^2	LQA (ppm)	MQA (ppm)
H_2	2.4	37.192	-15.906					0.9999	12-16	--
CO	6.2	0.1474	-5.7033					1.0000	<7.3	~1400

Both fits are for low cal gas, and as a result are only valid up to 1,000 ppm

Area Calibration Parameters for FID Med Signal

Gas	Retention Time (min)	a	m	b	σ_m^2	σ_b^2	σ_{mb}^2	RMSE (ppm)	R^2	LQA (ppm)	MQA (ppm)
H_2	2.4	--	36.825	2.6655					1.0000		
CO	6.2	0.0019	2.2834	62.405					0.9984		

These are taken from the combined H_2 and high-cal gas CO fits.

Calibration Graphs for High FID Sensitivity:

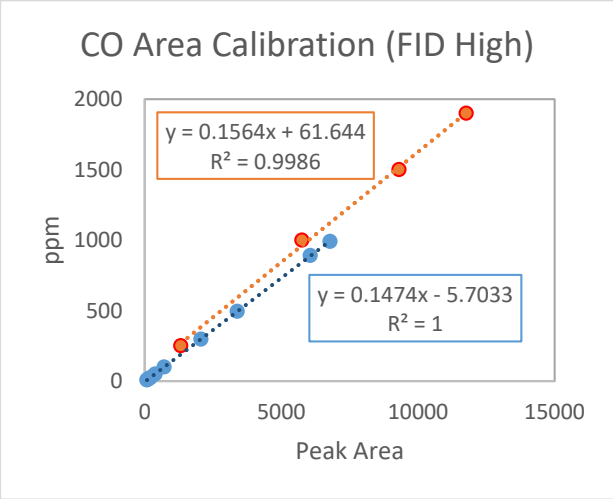

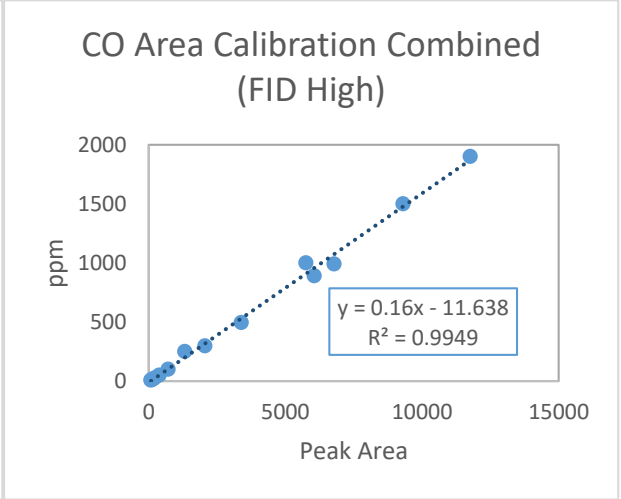

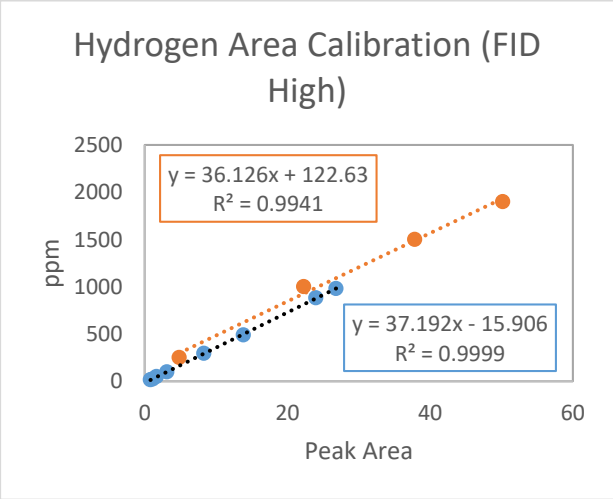

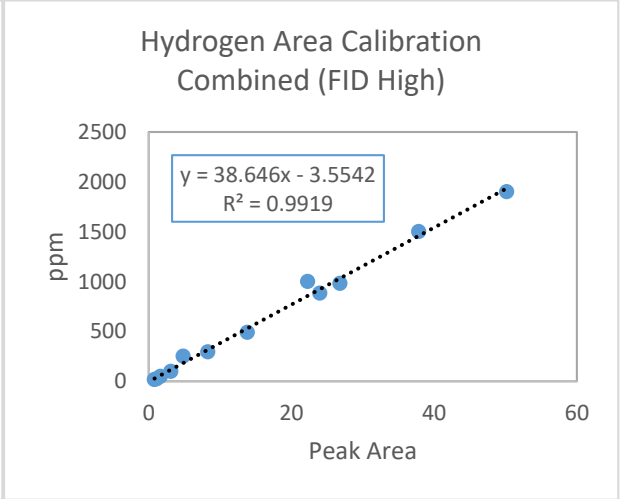

Fit for data points below 50 ppm CO: [CO] (ppm) = 0.13903×Peak Area – 4.12485

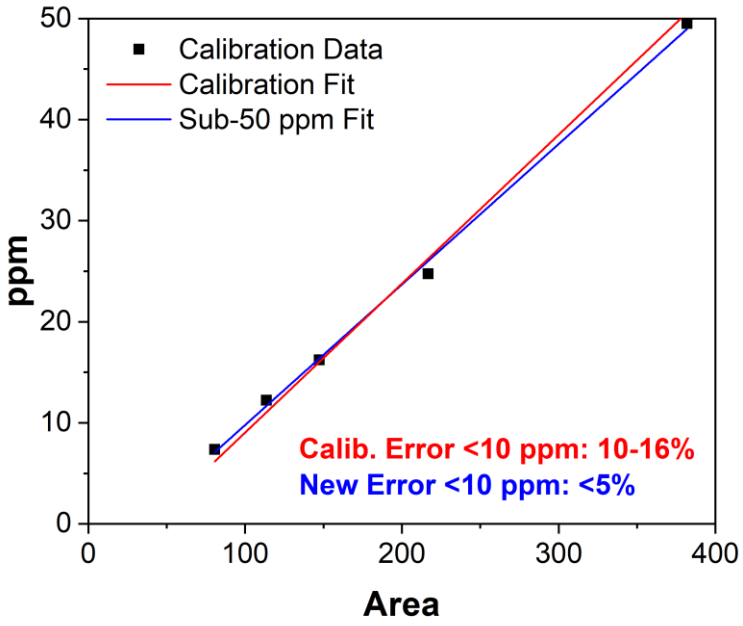

Calibration Graphs for Medium FID Sensitivity:

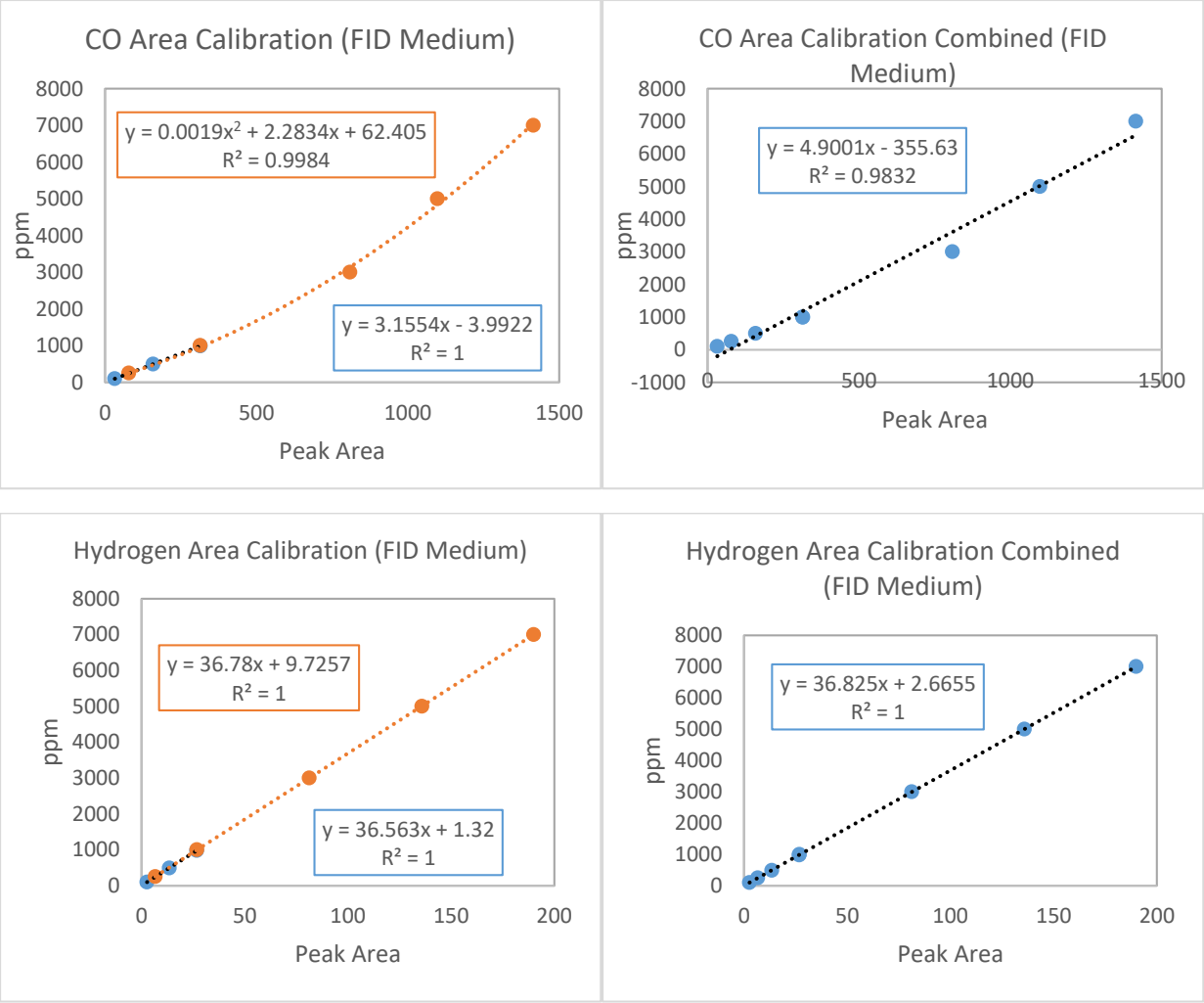

Typical gas chromatogram:

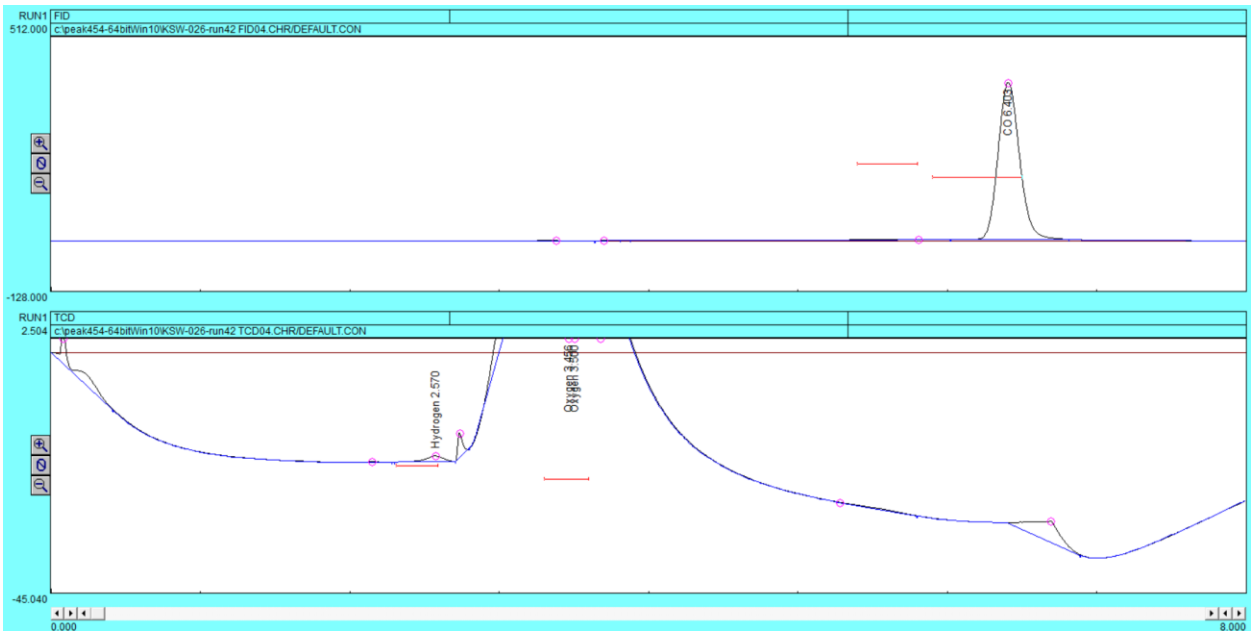

S.8.1.1 Calculating Partial Current from GC Data

GC peak areas were converted to parts-per-million (ppm) according to the procedure above. Once these values were known, they could be converted to partial current by:

$$ppm \times \frac{moles\ product/total\ moles}{1{,}000{,}000\ ppm} \times \frac{1\ total\ mol}{22.4\ std.L} \times \frac{1\ std.L}{1000\ scc} \times (flowrate)\ sccm \times \frac{1\ minute}{60\ sec} \times \frac{n\ moles\ e^-}{1\ mole\ product} \times \frac{96485.3\ C}{1\ mol\ e^-} \times \frac{1\ A}{1\ C/s} \times \frac{1000\ mA}{1\ A} = Partial\ Current\ (mA)$$

For example, for n = 2 (CO) and flowrate = 10 sccm, the conversion is 1 ppm = 1.436×10^{-3} mA.

S.8.2 Proton NMR for Liquid CO_2RR Products

^{1}H NMR was used to interrogate the formation of liquid-phase CO_2 reduction products such as methanol, ethanol, and formate. The procedure used to do this was taken from Kuhl et al.[10]

In short, samples were prepared by combining 700 µL of the bicarbonate catholyte with 35 µL standard solution containing 10 mM DMSO, 50 mM phenol in D_2O. Samples were then analyzed using a Varian 501 MHz NMR. Solvent suppression was conducted to dampen the water peak. (PreSat RF = 50, number of peaks = 1). The ^{1}H probe was manually tuned, lock was achieved on the D_2O in the sample, and gradient shimming was performed. Auto-gain was used, but phasing was performed manually. 36 transients were collected per sample.

Quantification was achieved by comparing the areas of the peaks of interest to those of the internal standards (phenol and DMSO – one standard on each side of the water peak to avoid issues due to phasing). To ensure that relaxation times did not convolute results, calibration curves were made for typically observed CO_2RR products such as formate and methanol (examples below). Detection limits for these methods were about 0.1 mM.

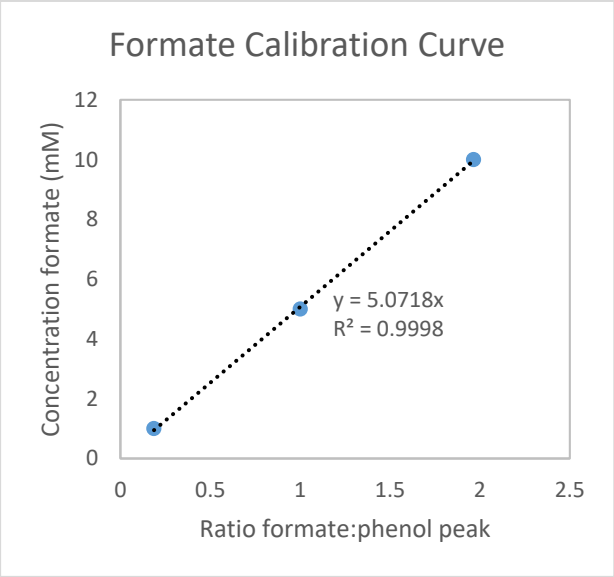

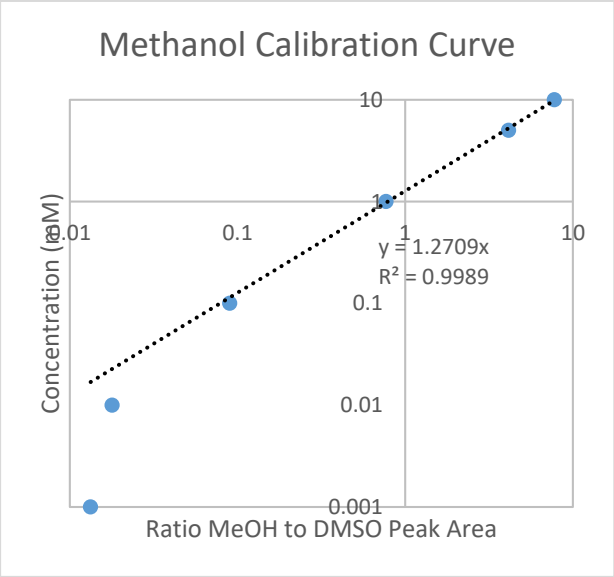

Blank NMR spectrum:

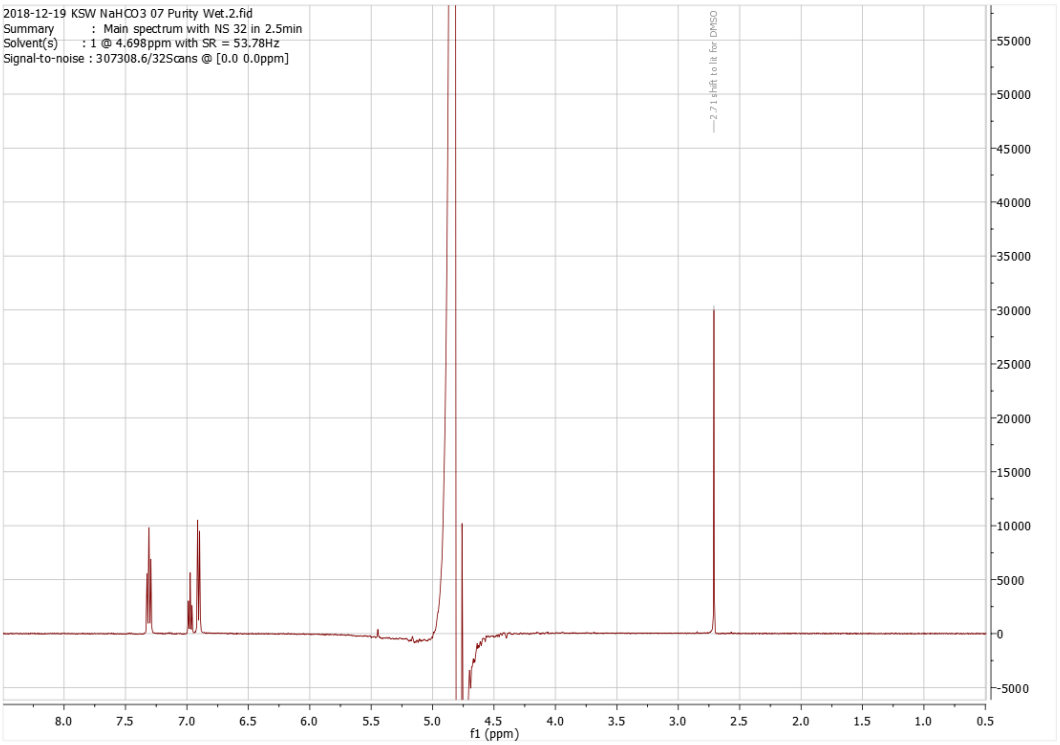

NMR spectrum post-electrolysis:

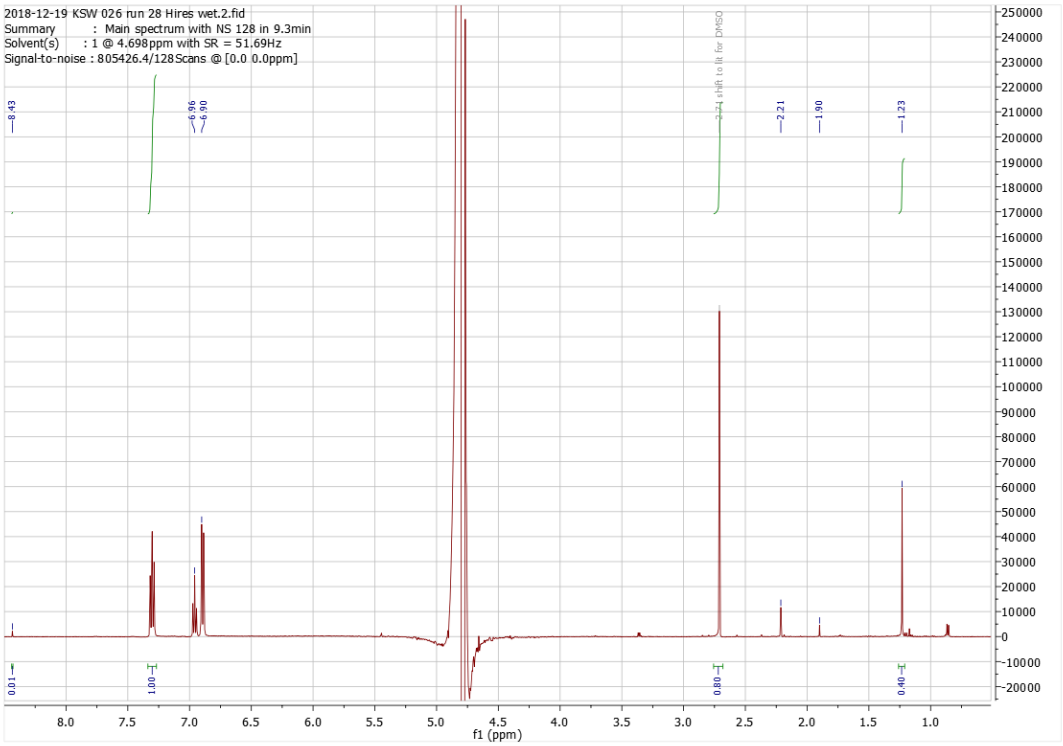

Note that a very small amount of formate (8.43 ppm above) was generated from Au, but not enough to contribute significantly to accounting for Faradaic efficiency. In addition, a negligible peak in the alcohols portion of the spectrum was present. The remaining peaks are likely acetone and hydrocarbon residues from the electrochemical cell itself.

S.8.3 UV-visible Quantification of Hydrogen Peroxide

Electrolytes were tested for hydrogen peroxide using a colorimetric assay.[11] 1 mL of electrolyte from a test having passed over 50 C of charge (16 hour test on gold around -0.7 V vs. RHE, flowing 5.0 sccm CO_2 and 5 sccm O_2 through 0.1 M $NaHCO_3$; charge toward ORR roughly 15 C) was combined with 1 mL of a stock solution containing 2.4 mM ammonium molybdate tetrahydrate and 0.5 M H_2SO_4 in Milli-Q®. The resulting solution appeared yellow in the presence of hydrogen peroxide. This solution was analyzed using an Ocean Optics spectrophotometer with a Flame-S-UV-Vis detector and a DH-mini-UV-Vis-NIR light source. The absorbance was scanned at wavelengths from 200 to 800 nm, and the absorbance at 370 nm was used to quantify peroxide. A blank bicarbonate solution spiked with the ammonium molybdate standard was used to zero the instrument prior to every acquisition. The calibration curve provided here has been constructed by JHM. A single data point with a known concentration of 5 mM H_2O_2 was used to check if this calibration curve, which is valid for detecting peroxide in water, was also valid for bicarbonate

solutions. The data point deviated less than 50% from the given curve, so a similar quantification limit is expected. No peroxide was observed.

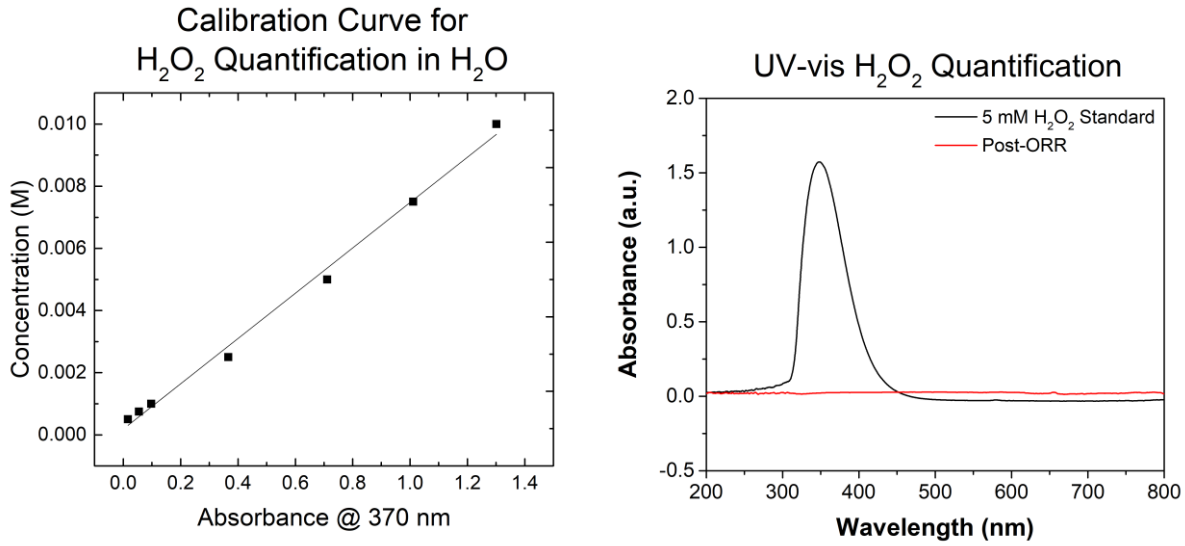

Figure S10. Peroxide quantification calibration curve and test confirming lack of peroxide generation.

Calibration equation: $(7.284\times10^{-3}) \times Abs_{370} + 0.190\times10^{-3}$ = concentration (M)

S.9 Discussion – Effect of O_2 at Lower Overpotentials

It should be noted that at potentials closer to the linear Tafel regime, a small but consistent downward trend in HER and CO_2RR was observed as more oxygen was added to the cell. This small downward trend is reflected in the consistently lower CO_2RR current densities obtained for all mechanistic tests in the main text. It is possible that this small downward trend is caused by the fact that ORR contributes a much higher percentage of the overall current density achieved at lower overpotentials, leading to a number of effects including an increase in pH in the vicinity of the electrode with large amounts of ORR taking place.

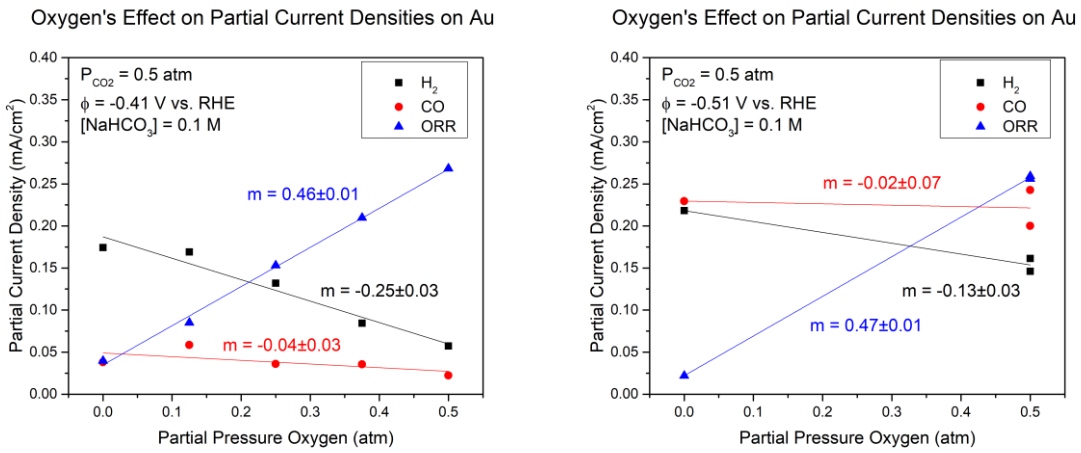

Figure S11. Effect of P_{O2} in gas feed on CO_2 reduction and HER at less reductive potentials than those discussed in the main text: -0.82 V vs. SHE and -0.92 V vs. SHE.

S.10 Discussion – CO_2RR Current Decay on Gold

It should be noted that a persistent observation during tests on gold was that CO_2RR currents decreased over time. This is consistent with observations from the literature regarding time-variance in currents and selectivities on polycrystalline Au.[12] A full treatment has been given to what we believe to be the cause this phenomenon: trace impurities in carbonate sources (Zn, Cu).[13] For this reason, only early-time-averaged data points (t = 20, 30, and 40 min) were used to construct all correlations described herein. Each data point taken in this work was from a newly assembled electrochemical cell and newly polished gold foil. A sample of data points taken after 1 hour of electroreduction indicates that this does not affect conclusions drawn (e.g. with regard to the values of Tafel slopes), so long as the procedure for calculating the current densities toward particular reactions is consistent across all data points on a single plot.

S.11 Discussion – Kinetic Rate Laws for CO_2RR

Under typical CO_2RR conditions in this study – namely, ambient temperature and pressure – the form of the Tafel slope should be:

$$Tafel\ slope = \frac{59\ mV/dec}{n + q\beta}$$

where n is the number of pre-RDS electron transfers, q is the number of electron transfers in the RDS (either 0 or 1 in almost all cases), and β is the symmetry factor – typically 0.5. A Tafel slope of 59 mV/dec implies that $n = 1$ and $q = 0$, or in other words that there is one electron transfer step prior to the RDS, and the RDS itself does not involve an electron transfer. This means that we need to write out a number of possibilities for what such a chemical step might be, as in the main text. Table 1 is reproduced below for reference.

Table S1. Reproduction of Table 1 for reference.

	RDS	Tafel Slope Form	Tafel Slope at 298 K, β = 0.5	Acidic Proton Order	P_{CO2} Order	KIE?
X.1	$CO_2 + \theta + e^- \rightleftharpoons \theta_{CO_2^{\bullet-}}$	$2.3RT/\beta F$	118	0	1	N
A.2	$\theta_{CO_2^{\bullet-}} + HCO_3^- \rightleftharpoons \theta_{COOH} + CO_3^{2-}$	$2.3RT/F$	59	1	1	Y
A.3	$\theta_{COOH} + e^- \rightleftharpoons \theta + CO + OH^-$	$2.3RT/(\beta+1)F$	39	0	1	N
B.2	$\theta_{CO_2^{\bullet-}} + H_2O \rightleftharpoons \theta_{COOH} + OH^-$	$2.3RT/F$	59	0	1	Y
B.3	$\theta_{COOH} + e^- \rightleftharpoons \theta + CO + OH^-$	$2.3RT/(\beta+1)F$	39	0	1	N
C.2*	$\theta_{CO_2^{\bullet-}} + [H^+] \rightleftharpoons \theta_{COOH}$	$2.3RT/F$	59		1	Y
C.3	$\theta_{COOH} + \theta \rightleftharpoons \theta_{CO} + \theta_{OH}$	$2.3RT/F$	59	0	1	N
C.4	$\theta_{CO} \rightleftharpoons \theta + CO$	$2.3RT/2F$	30	0	1	N
D.2	$\boldsymbol{\theta_{CO_2^{\bullet-}} + \theta \rightleftharpoons \theta_{CO} + \theta_{O^{\bullet-}}}$	$\boldsymbol{2.3RT/F}$	**59**	**0**	**1**	**N**
D.3	$\theta_{CO} \rightleftharpoons \theta + CO$	$2.3RT/2F$	30	0	1	N
E.2	$\boldsymbol{\theta_{CO_2^{\bullet-}} + CO_2 \rightleftharpoons \theta_{CO^+} + CO_3^{2-}}$	$\boldsymbol{2.3RT/F}$	**59**	**0**	**2**	**N**
E.3	$\theta_{CO^+} + e^- \rightleftharpoons \theta + CO$	$2.3RT/(\beta+1)F$	39	0	2	N
F.2*	$\theta_{CO_2^{\bullet-}} + [H^+] \rightleftharpoons \theta_{COOH}$	$2.3RT/F$	59		1	Y
F.3	$\theta_{COOH} \rightleftharpoons \theta_{CO^+} + OH^-$	$2.3RT/F$	59	0	1	N
F.4	$\theta_{CO^+} + e^- \rightleftharpoons \theta + CO$	$2.3RT/(\beta+1)F$	39	0	1	N
G.1†	$HCO_3^- + \theta + e^- \rightleftharpoons \theta_H + CO_3^{2-}$					
G.2	$\theta_{CO_2^{\bullet-}} + \theta_H \rightleftharpoons \theta_{COOH^-} + \theta$	$2.3RT/F$	59‡	0	1	Y
G.3	$\boldsymbol{\theta_{COOH^-} \rightleftharpoons \theta + CO + OH^-}$	$\boldsymbol{2.3RT/F}$	**59‡**	**0**	**1**	**N**
H.2	$\boldsymbol{\theta_{CO_2^{\bullet-}} + \gamma \rightleftharpoons \theta + \gamma_{CO_2^{\bullet-}}}$	$\boldsymbol{2.3RT/F}$	**59**	**0**	**1**	**N**
H.n◊	…					

After collecting kinetic data and narrowing down the list of possible RDSs, the remaining candidates include: (D.2) a vacant surface site could accept an $O^{\bullet -}$ atom, leaving a cationic CO adsorbate; (E.2) CO_2 could accept an $O^{\bullet -}$ atom, leaving a cationic CO adsorbate; (G.3) CO desorption under certain circumstances may be consistent with the given data; or (H.2) $\theta_{CO_2^{\bullet -}}$ could rearrange in a distinct chemical step on the surface before undergoing subsequent chemistry. Note that step G.2 has been excluded on the grounds of lack of observable KIE. While surface metal motions may be implicated in the vibrational modes of adsorbed protons – which may in turn dampen any observed KIE – it has been shown both theoretically[14] and experimentally[15] that KIEs from adsorbed species may be observed. Therefore, it is likely from KIE data that step G.2 is not the RDS.

D.2 and E.2 are regarded as unlikely mechanisms. In the case of D.2, the presence of $O^{\bullet -}$ adsorbate on gold has not to the authors' knowledge been described (although it has been seen on earlier transition metals and predicted for oxides of silver),[16,17] and may imply that gold is acting as the cation for $O^{\bullet -}$ – in other words, that a gold oxide is forming. Gold is not a very oxophilic metal, and at such reductive potentials as studied here, we are well within the stability window of Au^0.[18] In the case of E.2, the sudden formation of opposite charges without a concurrent electron transfer likely has quite a low probability; and, once again, this mechanism invokes an intermediate (θ_{CO+}) which seems only to have been described in metal complexes rather than on surfaces.[19,20]

In the case of CO desorption (G.3), such a step mathematically remains a candidate for the RDS if the two electrons involved in CO_2 reduction occur in parallel. However, such a mechanism also requires invoking the unlikely intermediate θ_{COOH-}, which can in principle exist, but only if drawn with a carbon radical. Further, the electron pushing required to finally achieve CO and OH^- evolution from this adsorbate is also dubious. Unfortunately, testing such an unlikely mechanistic step is also difficult – we do not believe that P_{CO} dependence studies necessarily probe the possibility that such a step is the RDS, as adding CO to the feed of a CO_2RR cell may modulate the bulk concentration of CO, but will likely not affect the concentration of CO at the electrode surface. This is because the activity of CO is already quite high (although not unity) in the vicinity of CO-containing bubbles at the surface.

It is of course possible, however, that the chemical step is merely a surface rearrangement of the $CO_2^{\bullet -}$ adsorbate (H.2). Because it has been shown that grain boundary sites are more active for CO_2 reduction,[21] it seems reasonable to suggest that certain sites are required for further chemistry to proceed on gold surfaces, and consequently that the diffusion of $CO_2^{\bullet -}$ to such sites could be the bottleneck in CO production. This hypothesis would require spectroscopic investigation.

Below we derive many of the kinetic rate laws which give rise to the kinetic parameters tabulated in Table 1 of the main text.

S.11.1 – Step A.2 as RDS

The first possibility considered in the text is that bicarbonate in solution, with a pK_a of 10.3 (therefore a better proton donor than water, with pK_a of 14.0), is donating a proton to adsorbed $CO_2^{-\cdot}$. We can write out the following elementary steps in such a mechanism, describing all steps other than the RDS as being in equilibrium:

A.1 $$CO_2 + \theta + e^- \rightleftharpoons \theta_{CO_2^-}$$

A.2 $$\theta_{CO_2^-} + HCO_3^- \rightarrow \theta_{COOH} + CO_3^{2-}$$

A.3 $$\theta_{COOH} + e^- \rightleftharpoons \theta + CO + OH^-$$

From A.2 being rate-limiting, we can assert that the following is true about the rate:

$$rate = k_{A2}\theta_{CO_2^-}[HCO_3^-]$$

Note that the rate constant k_{A2} is an agglomerate variable standing in for the Arrhenius kinetics of the reaction absent any potential driving force, i.e.:

$$k_{A2} = k_{A2,0}\exp\left(-\frac{E^0_{a,A2}}{RT}\right)$$

Note also that in the derivation of Butler-Volmer from basic kinetics principles, we are left with an expression that is exponentially dependent on φ, the absolute potential – not on overpotential.

While bicarbonate concentration is known in principle, the expression for the surface coverage of $CO_2^{-\cdot}$ must be calculated using the equilibrium expressions for steps A.1 and A.3:

$$K_{A1} = \frac{\theta_{CO_2^-}}{\theta[CO_2]\exp\left(\frac{-F\Phi}{RT}\right)} \quad \rightarrow \quad \theta_{CO_2^-} = K_{A1}\theta[CO_2]\exp\left(\frac{-F\Phi}{RT}\right)$$

$$K_{A3} = \frac{\theta[CO][OH^-]}{\theta_{COOH}\exp\left(\frac{-F\Phi}{RT}\right)} \quad \rightarrow \quad \theta_{COOH} = \frac{\theta[CO][OH^-]}{K_{A3}\exp\left(\frac{-F\Phi}{RT}\right)}$$

Henceforth, for simplicity, we will make a change of variables, substituting lowercase φ for the quantity –FΦ/RT.

We also have the site balance relationship:

$$\theta + \theta_{CO_2^-} + \theta_{COOH} = 1$$

Substituting,

$$\theta + K_{A1}\theta[CO_2]\exp(\phi) + \frac{\theta[CO][OH^-]}{K_{A3}\exp(\phi)} = 1$$

Isolating θ,

$$\theta = \frac{1}{1 + K_{A1}[CO_2]\exp(\phi) + \frac{[CO][OH^-]}{K_{A3}\exp(\phi)}}$$

Substituting back into the expression for the CO_2^- radical:

$$\theta_{CO_2^-} = \frac{K_{A1}[CO_2]\exp(\phi)}{1 + K_{A1}[CO_2]\exp(\phi) + \frac{[CO][OH^-]}{K_{A3}\exp(\phi)}}$$

Therefore the rate expression becomes:

$$rate = \frac{k_{A2}[HCO_3^-]K_{A1}[CO_2]\exp(\phi)}{1 + K_{A1}[CO_2]\exp(\phi) + \frac{[CO][OH^-]}{K_{A3}\exp(\phi)}}$$

In order to retain the exp(φ) term in the numerator and remain in line with the experimentally obtained Tafel slope, we must be in the limit of low adsorbate coverage (i.e. the dominant term in the denominator should be 1). Therefore,

$$rate = k_{A2}K_{A1}[HCO_3^-][CO_2]\exp(\phi)$$

This expression is 1st order in bicarbonate concentration as well as CO_2 concentration. Thus we can directly test this mechanism by assessing the order dependence of the rate with respect to bicarbonate and CO_2. Notably, if we instead wrote step A.3 as generating a θ_{CO} rather than CO directly, there would be one surface coverage term not containing exp(φ), meaning this limit of coverage could also hold true. This would result in a rate expression of

$$rate = \frac{k_{A2}K_{A1}K_{A4}[HCO_3^-][CO_2]\exp(\phi)}{[CO]}$$

which would additionally be inversely dependent upon CO concentration in solution. This argument holds true for many of the other dissociative steps to follow, but will not be discussed in depth.

Regarding the feasibility of the main-text conclusions – upon much thought regarding the mechanism, it seems fairly reasonable that bicarbonate, as a negatively charged species, would not be able to easily approach the negatively polarized electrode to conduct chemistry there. Electrostatic repulsion may in fact dictate that while there is a 3.7-order-of-magnitude driving force for bicarbonate to act as a proton donor (over water) in this context (partially negated by a 2.7-order-of-magnitude greater abundance of water than bicarbonate), still bicarbonate may have a difficult time participating in cathodic surface reactions. We investigate the possibility of water as the proton donor in S.11.3 below.

S.11.2 – Step B.2 as RDS

For mechanism B, the elementary steps are:

B.1 $$CO_2 + \theta + e^- \rightleftharpoons \theta_{CO_2^-}$$

B.2 $$\theta_{CO_2^-} + H_2O \rightarrow \theta_{COOH} + OH^-$$

B.3 $$\theta_{COOH} + e^- \rightleftharpoons \theta + CO + OH^-$$

The rate law is then:

$$rate = k_{B2}\theta_{CO_2^-}[H_2O]$$

Equilibria B.1 and B.3 give us:

$$K_{B1} = \frac{\theta_{CO_2^-}}{\theta[CO_2]\exp(\phi)} \quad \rightarrow \quad \theta_{CO_2^-} = K_{B1}\theta[CO_2]\exp(\phi)$$

$$K_{B3} = \frac{\theta[CO][OH^-]}{\theta_{COOH}\exp(\phi)} \quad \rightarrow \quad \theta_{CO^+} = \frac{\theta[CO][OH^-]}{K_{B3}\exp(\phi)}$$

We also have the site balance relationship:

$$\theta + \theta_{CO_2^-} + \theta_{COOH} = 1$$

Substituting,

$$\theta + K_{B1}\theta[CO_2]\exp(\phi) + \frac{\theta[CO][OH^-]}{K_{B3}\exp(\phi)} = 1$$

Isolating θ,

$$\theta = \frac{1}{1 + K_{B1}[CO_2]\exp(\phi) + \frac{[CO][OH^-]}{K_{B3}\exp(\phi)}}$$

Substituting back into the expression for the CO_2^- radical:

$$\theta_{CO_2^-} = \frac{K_{B1}[CO_2]\exp(\phi)}{1 + K_{B1}[CO_2]\exp(\phi) + \frac{[CO][OH^-]}{K_{B3}\exp(\phi)}}$$

Therefore the rate expression becomes:

$$rate = \frac{k_{B2}K_{B1}[CO_2][H_2O]\exp(\phi)}{1 + K_{B1}[CO_2]\exp(\phi) + \frac{[CO][OH^-]}{K_{B3}\exp(\phi)}}$$

In the low-coverage limit:

$$rate = k_{B2}K_{B1}[CO_2][H_2O]\exp(\phi)$$

This expression is 1st order in CO_2 concentration, and also in water. Because water is the solvent, there is no easy way to test the mechanism by varying the availability of the reactants. Therefore we are left to test this possibility with the kinetic isotope effect, as described previously.

S.11.3 – Step C.3 as RDS

For mechanism C derivation, we will assume water to be the proton donor; thus, the elementary steps are:

C.1 $$CO_2 + \theta + e^- \rightleftharpoons \theta_{CO_2^-}$$

C.2 $$\theta_{CO_2^-} + H_2O \rightarrow \theta_{COOH} + OH^-$$

C.3 $$\theta_{COOH} + \theta \rightleftharpoons \theta_{CO} + \theta_{OH}$$

C.4 $$\theta_{CO} \rightleftharpoons \theta + CO$$

C.5 $$\theta_{OH} + e^- \rightleftharpoons \theta + OH^-$$

The rate law is then:

$$rate = k_{C3}\theta_{COOH}\theta$$

Equilibria C.1, C.2, C.4, and C.5 give us:

$$K_{C1} = \frac{\theta_{CO_2^-}}{\theta[CO_2]\exp(\phi)} \quad \rightarrow \quad \theta_{CO_2^-} = K_{C1}\theta[CO_2]\exp(\phi)$$

$$K_{C2} = \frac{\theta_{COOH}[OH^-]}{\theta_{CO_2^-}[H_2O]} \quad \rightarrow \quad \theta_{COOH} = \frac{K_{C1}K_{C2}\theta[CO_2][H_2O]\exp(\phi)}{[OH^-]}$$

$$K_{C4} = \frac{\theta[CO]}{\theta_{CO}} \quad \rightarrow \quad \theta_{CO} = \frac{\theta[CO]}{K_{C4}}$$

$$K_{C5} = \frac{\theta[OH^-]}{\theta_{OH}\exp(\phi)} \quad \rightarrow \quad \theta_{OH} = \frac{\theta[OH^-]}{K_{C5}\exp(\phi)}$$

We also have the site balance relationship:

$$\theta + \theta_{CO_2^-} + \theta_{COOH} + \theta_{CO} + \theta_{OH} = 1$$

Substituting,

$$\theta + K_{C1}\theta[CO_2]\exp(\phi) + \frac{K_{C1}K_{C2}\theta[CO_2][H_2O]\exp(\phi)}{[OH^-]} + \frac{\theta[CO]}{K_{C4}} + \frac{\theta[OH^-]}{K_{C5}\exp(\phi)} = 1$$

Isolating θ,

$$\theta = \frac{1}{1 + K_{C1}[CO_2]\exp(\phi) + \frac{K_{C1}K_{C2}[CO_2][H_2O]\exp(\phi)}{[OH^-]} + \frac{[CO]}{K_{C4}} + \frac{[OH^-]}{K_{C5}\exp(\phi)}}$$

Substituting back into the expression for COOH:

$$\theta_{COOH} = \frac{K_{C1}K_{C2}[CO_2][H_2O]\exp(\phi)}{[OH^-]\left(1 + K_{C1}[CO_2]\exp(\phi) + \frac{K_{C1}K_{C2}[CO_2][H_2O]\exp(\phi)}{[OH^-]} + \frac{[CO]}{K_{C4}} + \frac{[OH^-]}{K_{C5}\exp(\phi)}\right)}$$

Therefore the rate expression becomes:

$$rate = \frac{k_{C3}K_{C1}K_{C2}[CO_2][H_2O]\exp(\phi)}{[OH^-]\left(1 + K_{C1}[CO_2]\exp(\phi) + \frac{K_{C1}K_{C2}[CO_2][H_2O]\exp(\phi)}{[OH^-]} + \frac{[CO]}{K_{C4}} + \frac{[OH^-]}{K_{C5}\exp(\phi)}\right)^2}$$

In the low-coverage limit:

$$rate = \frac{k_{C3}K_{C1}K_{C2}[CO_2][H_2O]\exp(\phi)}{[OH^-]}$$

This may in a sense be interpreted as an expression at least first-order in protons, in which case the mechanism can be eliminated as a possibility. Certainly surface pH should affect the rate of a reaction under such control; however, tests to probe pH effects are inextricably convoluted with other aspects of the solution chemistry, and would have to be confirmed with efforts to model surface pH under reaction conditions.

S.11.4 – Step D.2 as RDS

For mechanism D, the elementary steps are:

D.1 $$CO_2 + \theta + e^- \rightleftharpoons \theta_{CO_2^-}$$

D.2 $$\theta_{CO_2^-} + \theta \rightarrow \theta_{CO} + \theta_{O^-}$$

D.3 $$\theta_{CO} \rightleftharpoons \theta + CO$$

To complete the mechanism, O-atom anion adsorbates would have to undergo the following final step, or something adjacent:

D.4 $$\theta_{O^-} + HCO_3^- + e^- \rightleftharpoons \theta + OH^- + CO_3^{2-}$$

We have the following rate expression in the case of D.2 as the RDS:

$$rate = k_{D2}\theta_{CO_2^-}\theta$$

Equilibria D.1, D.3, and D.4 give us:

$$K_{D1} = \frac{\theta_{CO_2^-}}{\theta[CO_2]\exp(\phi)} \quad \rightarrow \quad \theta_{CO_2^-} = K_{D1}\theta[CO_2]\exp(\phi)$$

$$K_{D3} = \frac{\theta[CO]}{\theta_{CO}} \quad \rightarrow \quad \theta_{CO} = \frac{\theta[CO]}{K_{D3}}$$

$$K_{D4} = \frac{\theta[OH^-][CO_3^{2-}]}{\theta_{O^-}[HCO_3^-]\exp(\phi)} \quad \rightarrow \quad \theta_{O^-} = \frac{\theta[OH^-][CO_3^{2-}]}{K_{D4}[HCO_3^-]\exp(\phi)}$$

We also have the site balance relationship:

$$\theta + \theta_{CO_2^-} + \theta_{CO} + \theta_{O^-} = 1$$

Substituting,

$$\theta + K_{D1}\theta[CO_2]\exp(\phi) + \frac{\theta[CO]}{K_{D3}} + \frac{\theta[OH^-][CO_3^{2-}]}{K_{D4}[HCO_3^-]\exp(\phi)} = 1$$

Isolating θ,

$$\theta = \frac{1}{1 + K_{D1}[CO_2]\exp(\phi) + \frac{[CO]}{K_{D3}} + \frac{[OH^-][CO_3^{2-}]}{K_{D4}[HCO_3^-]\exp(\phi)}}$$

Substituting back into the expression for the CO_2^- radical:

$$\theta_{CO_2^-} = \frac{K_{D1}[CO_2]\exp(\phi)}{1 + K_{D1}[CO_2]\exp(\phi) + \frac{[CO]}{K_{D3}} + \frac{[OH^-][CO_3^{2-}]}{K_{D4}[HCO_3^-]\exp(\phi)}}$$

Therefore the rate expression becomes:

$$rate = \frac{k_{D2}K_{D1}[CO_2]\exp(\phi)}{\left(1 + K_{D1}[CO_2]\exp(\phi) + \frac{[CO]}{K_{D3}} + \frac{[OH^-][CO_3^{2-}]}{K_{D4}[HCO_3^-]\exp(\phi)}\right)^2}$$

In the low-coverage limit:

$$rate = k_{D2}K_{D1}[CO_2]\exp(\phi)$$

Also, in the limit of high CO coverage, the same Tafel slope holds, while there is a $[CO]^{-2}$ dependence of the rate.

S.11.5 – Step E.2 as RDS

We apply analysis in much the same form for subsequent mechanistic possibilities. For mechanism E, the RDS possibility is step E.2, so that the elementary steps are:

E.1 $$CO_2 + \theta + e^- \rightleftharpoons \theta_{CO_2^-}$$

E.2 $$\theta_{CO_2^-} + CO_2 \rightarrow \theta_{CO^+} + CO_3^{2-}$$

E.3 $$\theta_{CO^+} + e^- \rightleftharpoons \theta + CO$$

The rate law is then:

$$rate = k_{E2}\theta_{CO_2^-}[CO_2]$$

Equilibria E.1 and E.3 give us:

$$K_{E1} = \frac{\theta_{CO_2^-}}{\theta[CO_2]\exp(\phi)} \quad \rightarrow \quad \theta_{CO_2^-} = K_{E1}\theta[CO_2]\exp(\phi)$$

$$K_{E3} = \frac{\theta[CO]}{\theta_{CO^+}\exp(\phi)} \quad \rightarrow \quad \theta_{CO^+} = \frac{\theta[CO]}{K_{E3}\exp(\phi)}$$

We also have the site balance relationship:

$$\theta + \theta_{CO_2^-} + \theta_{CO^+} = 1$$

Substituting,

$$\theta + K_{E1}\theta[CO_2]\exp(\phi) + \frac{\theta[CO]}{K_{E3}\exp(\phi)} = 1$$

Isolating θ,

$$\theta = \frac{1}{1 + K_{E1}[CO_2]\exp(\phi) + \frac{[CO]}{K_{E3}\exp(\phi)}}$$

Substituting back into the expression for the CO_2^- radical:

$$\theta_{CO_2^-} = \frac{K_{E1}[CO_2]\exp(\phi)}{1 + K_{E1}[CO_2]\exp(\phi) + \frac{[CO]}{K_{E3}\exp(\phi)}}$$

Therefore the rate expression becomes:

$$rate = \frac{k_{E2}K_{E1}[CO_2]^2\exp(\phi)}{1 + K_{E1}[CO_2]\exp(\phi) + \frac{[CO]}{K_{E3}\exp(\phi)}}$$

In the low-coverage limit:

$$rate = k_{E2}K_{E1}[CO_2]^2 \exp(\phi)$$

This expression is 2nd order in CO_2 concentration. Thus we can directly test this mechanism by assessing the order dependence of the rate with respect to CO_2.

S.11.6 – Step F.3 as RDS

For mechanism F, the elementary steps are:

F.1 $$CO_2 + \theta + e^- \rightleftharpoons \theta_{CO_2^-}$$

F.2 $$\theta_{CO_2^-} + H_2O \rightarrow \theta_{COOH} + OH^-$$

F.3 $$\theta_{COOH} \rightleftharpoons \theta_{CO^+} + OH^-$$

F.4 $$\theta_{CO^+} + e^- \rightleftharpoons \theta + CO$$

The rate law is then:

$$rate = k_{F3}\theta_{COOH^-}$$

Equilibria F.1, F.2, and F.4 give us:

$$K_{F1} = \frac{\theta_{CO_2^-}}{\theta[CO_2]\exp(\phi)} \quad \rightarrow \quad \theta_{CO_2^-} = K_{F1}\theta[CO_2]\exp(\phi)$$

$$K_{F2} = \frac{\theta_{COOH}[OH^-]}{\theta_{CO_2^-}[H_2O]} \quad \rightarrow \quad \theta_{COOH} = \frac{K_{F2}K_{F1}\theta[CO_2][H_2O]\exp(\phi)}{[OH^-]}$$

$$K_{F4} = \frac{\theta[CO]}{\theta_{CO^+}\exp(\phi)} \quad \rightarrow \quad \theta_{CO^+} = \frac{\theta[CO]}{K_{F4}\exp(\phi)}$$

We also have the site balance relationship:

$$\theta + \theta_{CO_2^-} + \theta_{COOH} + \theta_{CO^+} = 1$$

Substituting,

$$\theta + K_{F1}\theta[CO_2]\exp(\phi) + \frac{K_{F2}K_{F1}\theta[CO_2][H_2O]\exp(\phi)}{[OH^-]} + \frac{\theta[CO]}{K_{F4}\exp(\phi)} = 1$$

Isolating θ,

$$\theta = \frac{1}{1 + K_{F1}[CO_2]\exp(\phi) + \frac{K_{F2}K_{F1}[CO_2][H_2O]\exp(\phi)}{[OH^-]} + \frac{[CO]}{K_{F4}\exp(\phi)}}$$

Substituting back into the expression for $COOH^-$:

$$\theta_{COOH} = \frac{K_{F2}K_{F1}[CO_2][H_2O]\exp(\phi)}{[OH^-] + K_{F1}[CO_2][OH^-]\exp(\phi) + K_{F2}K_{F1}[CO_2][H_2O]\exp(\phi) + \frac{[CO][OH^-]}{K_{F4}\exp(\phi)}}$$

Therefore the rate expression becomes:

$$rate = \frac{k_{F3}K_{F2}K_{F1}[CO_2][H_2O]\exp(\phi)}{[OH^-] + K_{F1}[CO_2][OH^-]\exp(\phi) + K_{F2}K_{F1}[CO_2][H_2O]\exp(\phi) + \frac{[CO][OH^-]}{K_{F4}\exp(\phi)}}$$

In the low-coverage limit:

$$rate = \frac{k_{F3}K_{F2}K_{F1}[CO_2][H_2O]\exp(\phi)}{[OH^-]}$$

This may in a sense be interpreted as an expression at least first-order in protons, in which case the mechanism can be eliminated as a possibility. Certainly surface pH should affect the rate of a reaction under such control; however, tests to probe pH effects are inextricably convoluted with other aspects of the solution chemistry, and would have to be confirmed with efforts to model surface pH under reaction conditions.

S.11.7 – Step G.2/G.3 as RDS

For mechanism G, the elementary steps are:

G.1 $$CO_2 + \theta + e^- \rightleftharpoons \theta_{CO_2^-}$$
$$HCO_3^- + \theta + e^- \rightleftharpoons \theta_H + CO_3^{2-}$$

G.2 $$\theta_{CO_2^-} + \theta_H \rightarrow \theta_{COOH^-} + \theta$$

G.3 $$\theta_{COOH^-} \rightleftharpoons \theta + CO + OH^-$$

Here there is necessary adsorption of H to the surface prior to the CO_2RR RDS. In principle, the donor for this proton could also be water, and the adsorbed H could also divert toward HER. Depending on the HER mechanism, the subsequent step may either be the Tafel or Heyrovsky generation of H_2:

Tafel $$2\theta_H \rightleftharpoons 2\theta + H_2$$

Heyrovsky $$\theta_H + HCO_3^- + e^- \rightleftharpoons \theta + H_2 + CO_3^{2-}$$

It has been shown in other works' Supporting Information that using the initial H adsorption as the equilibrium expression for the coverage θ_H leads to Tafel slopes not consistent with our experimental data (30 mV/dec).[22] If, however, the Volmer step (H adsorption) is the RDS of HER, and not truly in equilibrium, then the equilibrium expression that holds true is either the Tafel or Heyrovsky relation. We will derive here the case in which the equilibrium expression for θ_H is obtained through the Tafel step equilibrium.

$$rate = k_{D2}\theta_{CO_2^-}\theta_H$$

Equilibria G.1, G.3, and the Tafel step give us:

$$K_{G1} = \frac{\theta_{CO_2^-}}{\theta[CO_2]\exp(\phi)} \quad \rightarrow \quad \theta_{CO_2^-} = K_{G1}\theta[CO_2]\exp(\phi)$$

$$K_{G3} = \frac{\theta[CO][OH^-]}{\theta_{COOH^-}} \quad \rightarrow \quad \theta_{COOH^-} = \frac{\theta[CO][OH^-]}{K_{G3}}$$

$$K_{GT} = \frac{\theta^2[H_2]}{\theta_H^2} \quad \rightarrow \quad \theta_H = \sqrt{\frac{[H_2]}{K_{GT}}}\,\theta$$

We also have the site balance relationship:

$$\theta + \theta_{CO_2^-} + \theta_{COOH^-} + \theta_H = 1$$

Substituting,

$$\theta + K_{G1}\theta[CO_2]\exp(\phi) + \frac{\theta[CO][OH^-]}{K_{G3}} + \sqrt{\frac{[H_2]}{K_{GT}}}\,\theta = 1$$

Isolating θ,

$$\theta = \frac{1}{1 + K_{G1}[CO_2]\exp(\phi) + \frac{[CO][OH^-]}{K_{G3}} + \sqrt{\frac{[H_2]}{K_{GT}}}}$$

Substituting back into the expressions for the CO_2^- radical and H sites:

$$\theta_{CO_2^-} = \frac{K_{G1}[CO_2]\exp(\phi)}{1 + K_{G1}[CO_2]\exp(\phi) + \frac{[CO][OH^-]}{K_{G3}} + \sqrt{\frac{[H_2]}{K_{GT}}}}$$

$$\theta_H = \frac{\sqrt{\frac{[H_2]}{K_{GT}}}}{1 + K_{G1}[CO_2]\exp(\phi) + \frac{[CO][OH^-]}{K_{G3}} + \sqrt{\frac{[H_2]}{K_{GT}}}}$$

Therefore the rate expression becomes:

$$rate = \frac{k_{G2}K_{G1}[CO_2]\sqrt{\frac{[H_2]}{K_{GT}}}\exp(\phi)}{\left(1 + K_{G1}[CO_2]\exp(\phi) + \frac{[CO][OH^-]}{K_{G3}} + \sqrt{\frac{[H_2]}{K_{GT}}}\right)^2}$$

In the low-coverage limit:

$$rate = k_{G2}K_{G1}[CO_2]\sqrt{\frac{[H_2]}{K_{GT}}}\exp(\phi)$$

The unique thing about this mechanism is that it is 0.5-order in the concentration of H_2 gas. However, due to H_2's low solubility in water and relative abundance at the surface of the cathode, this mechanism is rather difficult to test by modulating P_{H2}.

It should also be noted that such a mechanism is additionally plausible by assuming separate types of adsorption sites for protons on the surface, in which case the following expression is obtained (γ = H adsorption site):

$$rate = \frac{k_{G2}K_{G1}[CO_2]\sqrt{\frac{[H_2]}{K_{GT}}}\exp(\phi)}{\left(1 + K_{G1}[CO_2]\exp(\phi) + \frac{[CO][OH^-]}{K_{G3}}\right)\left(1 + \sqrt{\frac{[H_2]}{K_{GT}}}\right)}$$

Moreover, Tafel slopes are still consistent with experiment even if the coverages of $COOH^-$ or H dominate in either case. However, this mechanism was excluded in the main text because it likely involves an observable KIE.

In the case of G.3 as the RDS, we have the rate:

$$rate = k_{G3}\theta_{COOH^-}$$

Equilibria G.1, G.2, and the Tafel step give us:

$$K_{G1} = \frac{\theta_{CO_2^-}}{\theta[CO_2]\exp(\phi)} \quad \rightarrow \quad \theta_{CO_2^-} = K_{G1}\theta[CO_2]\exp(\phi)$$

$$K_{GT} = \frac{\theta^2[H_2]}{\theta_H^2} \quad \rightarrow \quad \theta_H = \sqrt{\frac{[H_2]}{K_{GT}}}\,\theta$$

$$K_{G2} = \frac{\theta\theta_{COOH^-}}{\theta_{CO_2^-}\cdot\theta_H} \quad \rightarrow \quad \theta_{COOH^-} = K_{G1}K_{G2}\theta[CO_2]\sqrt{\frac{[H_2]}{K_{GT}}}\exp(\phi)$$

We also have the site balance relationship:

$$\theta + \theta_{CO_2^-\cdot} + \theta_{COOH^-} + \theta_H = 1$$

Substituting,

$$\theta + K_{G1}\theta[CO_2]\exp(\phi) + K_{G1}K_{G2}\theta[CO_2]\sqrt{\frac{[H_2]}{K_{GT}}}\exp(\phi) + \sqrt{\frac{[H_2]}{K_{GT}}}\,\theta = 1$$

Isolating θ,

$$\theta = \frac{1}{1 + K_{G1}[CO_2]\exp(\phi) + K_{G1}K_{G2}[CO_2]\sqrt{\frac{[H_2]}{K_{GT}}}\exp(\phi) + \sqrt{\frac{[H_2]}{K_{GT}}}}$$

Substituting back into the expressions for the $COOH^-$ sites:

$$\theta_{COOH^-} = \frac{K_{G1}K_{G2}[CO_2]\sqrt{\frac{[H_2]}{K_{GT}}}\exp(\phi)}{1 + K_{G1}[CO_2]\exp(\phi) + K_{G1}K_{G2}[CO_2]\sqrt{\frac{[H_2]}{K_{GT}}}\exp(\phi) + \sqrt{\frac{[H_2]}{K_{GT}}}}$$

Therefore the rate expression becomes:

$$rate = \frac{k_{G3}K_{G1}K_{G2}[CO_2]\sqrt{\frac{[H_2]}{K_{GT}}}\exp(\phi)}{1 + K_{G1}[CO_2]\exp(\phi) + K_{G1}K_{G2}[CO_2]\sqrt{\frac{[H_2]}{K_{GT}}}\exp(\phi) + \sqrt{\frac{[H_2]}{K_{GT}}}}$$

In the low-coverage limit:

$$rate = k_{G3}K_{G1}K_{G2}[CO_2]\sqrt{\frac{[H_2]}{K_{GT}}}\exp(\phi)$$

S.11.8 – Step H.2 as RDS

There are a number of post-RDS paths in mechanism H, so these have not been specified in the table, nor will they be specified here. However, it should follow from very similar math as applied above that the rearrangement of adsorbed $CO_2^{\bullet-}$ on the surface is a chemical step with a Tafel slope of 59 mV/dec, first-order dependence on CO_2, and no dependence on protons.

SI References

1 P. Lobaccaro, M. R. Singh, E. L. Clark, Y. Kwon, A. T. Bell and J. W. Ager, *Phys. Chem. Chem. Phys.*, 2016, **18**, 26777–26785.

2 A. J. Bard and L. R. Faulkner, *Electrochemical Methods*, Wiley, 2nd edn., 2001.

3 S. Weisenberger and A. Schumpe, *AIChE J.*, 1996, **42**, 298–300.

4 U. S. D. of Commerce, NIST Chemistry WebBook, http://webbook.nist.gov/chemistry/%0A.

5 H. Yoshida, K. Okuno and Y. Naruse, *J. Nucl. Sci. Technol.*, 1982, **19**, 578–586.

6 E. L. Clark, J. Resasco, A. Landers, J. Lin, L.-T. Chung, A. Walton, C. Hahn, T. F. Jaramillo and A. T. Bell, *ACS Catal.*, 2018, acscatal.8b01340.

7 S. J. Konopka and B. Mcduffie, *Anal. Chem.*, 1970, **42**, 1741–1746.

8 W. M. Deen, *Analysis of Transport Phenomena*, Oxford University Press, 2nd edn., 2011.

9 E. L. Cussler, *Diffusion: Mass Transfer in Fluid Systems (2nd Ed.)*, 1997.

10 K. P. Kuhl, E. R. Cave, D. N. Abram and T. F. Jaramillo, *Energy Environ. Sci.*, 2012, **5**, 7050–7059.

11 F. L. Silva, R. M. Reis, W. R. P. Barros, R. S. Rocha and M. R. V Lanza, 2014, **723**, 32–37.

12 Y. Chen, C. W. Li and M. W. Kanan, *J. Am. Chem. Soc.*, 2012, **134**, 19969–19972.

13 A. Wuttig and Y. Surendranath, *ACS Catal.*, 2015, **5**, 4479–4484.

14 T. N. Truong and D. G. Truhlar, *J. Chem. Phys.*, 1988, **88**, 6611.

15 M. Ojeda, A. Li, R. Nabar, A. U. Nilekar, M. Mavrikakis and E. Iglesia, *J. Phys. Chem. C*, 2010, **114**, 19761–19770.

16 V. A. Shvets and V. B. Kazansky, *J. Catal.*, 1972, **130**, 123–130.

17 E. V. Trushin and I. L. Zilberberg, *Chem. Phys. Lett.*, 2013, **560**, 37–41.

18 M. Pourbaix, *Atlas of Electrochemical Equilibria in Aqueous Solutions*, National Association of Corrosion Engineers, 1974.

19 A. S. Goldman and K. Krogh-Jespersen, *J. Am. Chem. Soc.*, 1996, **118**, 12159–12166.

20 Q. Xu, *Coord. Chem. Rev.*, 2002, **231**, 83–108.

21 R. G. Mariano, K. McKelvey, H. S. White and M. W. Kanan, *Science (80-.).*, 2017, **358**, 1187–1192.

22 A. Wuttig, Y. Yoon, J. Ryu and Y. Surendranath, *J. Am. Chem. Soc.*, 2017, **139**, 17109–17113.